

# **Influence of the Intramedullary Stem in Total Knee Arthroplasty**

**Sara Beatriz Marques Freitas**

Thesis to obtain the Master of Science Degree in

## **Biomedical Engineering**

Supervisor(s): Prof. João Orlando Marques Gameiro Folgado  
Prof. Luís Alberto Gonçalves de Sousa

### **Examination Committee**

Chairperson: Prof. Fernando Miguel Fernandes Simões  
Supervisor: Prof. Luís Alberto Gonçalves de Sousa  
Member of the Committee: Prof. João Manuel Pereira Dias  
Doutor Mário João Baptista Nunes de Mourão Gamelas

**October 2021**



Para os meus pais, Nuno e Daniela.  
Para a minha avó, Maria Conceição.



## **Preface**

The work presented in this thesis was performed at the Department of Mechanical Engineering (DEM) of Instituto Superior Técnico (Lisbon, Portugal), during the period September 2020-July 2021, under the supervision of Prof. João Folgado, Prof. Luís Sousa and Dr. Mário Gamelas.

## **Declaration**

I declare that this document is an original work of my own authorship and that it fulfills all the requirements of the Code of Conduct and Good Practices of the Universidade de Lisboa.



## Agradecimentos

Gostaria de agradecer aos meus orientadores, Professor Luís Sousa e Professor João Folgado, por toda a disponibilidade, apoio e orientação ao longo deste trabalho. Gostaria de agradecer também ao Professor Doutor Mário Gamelas, por toda a sua disponibilidade, em particular na fase inicial do trabalho, a nível da integridade anatómica dos modelos de Solidworks e ao Professor Carlos Quental, por todas as sugestões e pela sua disponibilidade para esclarecer dúvidas ao longo deste trabalho.

A nível pessoal, muitas pessoas passaram pelo meu caminho até este ponto, pelo que seria impossível agradecer a todos. No entanto, sinto-me na obrigação de referir algumas pessoas que sem as quais, o meu percurso não teria sido, certamente, tão feliz. Aos meus amigos, Diogo, Tiago, Joana, Constança, Zé e Miguel, com os quais partilhei os últimos anos. O vosso apoio e amizade foram fundamentais para mim nesta caminhada. Agradeço-vos a todos as memórias que comigo criaram, com a certeza que ainda criaremos muitas mais.

Quero agradecer à minha família, que sempre me apoiou e incentivou, não só ao longo deste trabalho, mas durante todo o meu percurso. Por todos os esforços e sacrifícios que fizeram para que pudesse chegar aqui, do fundo do meu coração, obrigada.

Aos meus pais em particular, queria fazer um agradecimento especial, pelo apoio incondicional que me deram durante toda a minha vida. Tive a sorte de crescer com a certeza de que, qualquer que fosse o meu caminho, estariam sempre ao meu lado, a apoiar-me e a incentivar-me. É verdadeiramente maravilhoso, quando os nossos pais são os nossos melhores amigos e maiores apoiantes. Por tudo o que me deram, sou eternamente grata. Espero que este trabalho, com o qual concluo este ciclo da minha vida, vos deixe orgulhosos. Da mesma forma, espero que saibam que tudo o que fizer, daqui em diante, será com o objetivo de honrar-vos e deixar-vos orgulhosos de mim.



## Resumo

A osteoartrite é responsável pela degradação progressiva da cartilagem articular do joelho. Em casos de degradação acentuada, a Artroplastia Total do Joelho é usada para restaurar a função e alinhamento da articulação do joelho. Esta é uma das cirurgias com maiores taxas de sucesso atualmente, com resultados notáveis a longo prazo. Ainda assim, complicações pós-operatórias podem ocorrer, resultando em cirurgias de revisão em que os componentes danificados são removidos e substituídos. Nas cirurgias de revisão, hastes intramedulares são introduzidas juntamente com os componentes protéticos primários, de forma a aumentar a sua fixação e estabilidade. O uso de modelos computacionais pode melhorar o desenho do implante e o planeamento pré-operatório da cirurgia, e consequentemente melhorar os resultados pós-operatórios.

O objectivo deste trabalho é analisar os efeitos que a introdução de uma haste endomedular tem nas forças e tensões a que o osso complementar fica sujeito, após uma cirurgia de revisão, com recurso a modelos computacionais e a análise de elementos finitos. Para tal, quatro modelos foram criados, com diferentes configurações de inserção de hastes. Foram aplicadas forças musculares, com o intuito de replicar o carregamento a que a prótese está sujeita. Vários casos de carga foram considerados, de acordo com as diferentes fases do ciclo de marcha.

Os resultados obtidos demonstram que a inserção de uma haste tibial afecta de forma insignificante a distribuição de tensões no fémur. Verificou-se também que, nos casos de inserção de haste femoral, as tensões a que o fémur está sujeito diminuíram, confirmando assim o efeito de stress shielding esperado.

**Palavras-chave:** Artroplastia Total do Joelho, cirurgia de revisão, haste intramedular, Análise de Elementos Finitos, Stress de Von Mises



## Abstract

Knee osteoarthritis is responsible for the progressive degradation of the knee articular cartilage. In serious cases, total knee arthroplasty is used to restore the function and alignment of the knee joint. TKA is one of the most successful and cost-effective surgeries in modern medicine, with remarkable long-term surgical outcomes. Nevertheless, it is possible for postoperative complications to occur, resulting in revision surgeries, where the damaged components are removed and replaced. In revision surgeries, intramedullary stems are introduced, along with the primary prosthetic components, in order to increase fixation and stability. The use of computational models can improve the design and preoperative planning of the TKA, and consequently improve the surgical outcome.

The main goal of this work is to analyze how the introduction of an intramedullary stem during revision surgery affects the forces and stresses acting on the complementary bone, through the use of computational models and finite element analysis. Therefore, four models were created, with different stem insertion configurations. Muscle forces were applied, so as to mimic the loading the prosthesis is subjected to. Several loading cases were considered, according to different phases of the walking gate cycle.

Results wise, the main conclusion of this study is that the insertion of a tibial stem, affects insignificantly the stress distributions in the femur. Furthermore, in the cases where a femoral stem was inserted, the femur stresses lowered, thus confirming the expected stress shielding effect.

**Keywords:** Total knee arthroplasty, revision surgery, stem, Finite Element Analysis, Von Mises stress



# Contents

Preface . . . . .	v
Declaration . . . . .	v
Acknowledgments . . . . .	vii
Resumo . . . . .	ix
Abstract . . . . .	xi
Contents . . . . .	xiv
List of Tables . . . . .	xiv
List of Figures . . . . .	xvi
Nomenclature . . . . .	xix
Acronyms . . . . .	xx
<b>1 Introduction</b>	<b>1</b>
1.1 Motivation and Goals . . . . .	1
1.2 Thesis Outline . . . . .	2
<b>2 Background</b>	<b>5</b>
2.1 Knee Joint . . . . .	5
2.1.1 Descriptive Terminology . . . . .	6
2.1.2 Synovial Joint . . . . .	7
2.1.3 Knee Joint Anatomy . . . . .	8
2.1.3.1 Femur . . . . .	9
2.1.3.2 Tibia and Fibula . . . . .	9
2.1.3.3 Patella . . . . .	10
2.1.3.4 Ligaments, Muscles and Tendons . . . . .	11
2.1.3.5 Menisci . . . . .	13
2.2 Knee Alignment . . . . .	14
2.2.1 Varus and Valgus Alignments . . . . .	15
2.3 Knee Joint Biomechanics . . . . .	15
2.3.1 Knee Joint Kinematics . . . . .	16
2.4 Total Knee Arthroplasty . . . . .	18
2.4.1 Indications and Contraindications . . . . .	18

2.4.2	Prosthesis Choice and Posterior Stabilized Fixed Bearing Knee Prosthesis . . . .	19
2.4.2.1	Primary TKA . . . . .	19
2.4.2.2	Revision TKA . . . . .	21
2.4.3	Epidemiology . . . . .	21
2.4.4	Primary Total Knee Arthroplasty Surgical Technique . . . . .	22
2.4.5	Complications . . . . .	24
2.4.6	Revision Total Knee Arthroplasty . . . . .	25
2.4.6.1	Revision Total Knee Arthroplasty Surgical Technique . . . . .	25
<b>3</b>	<b>Implementation</b>	<b>29</b>
3.1	Bone Images Acquisition . . . . .	29
3.2	Bone Segmentation Process . . . . .	30
3.3	Smoothing Process of the Segmentation Results . . . . .	32
3.4	Geometric Modelling and Assembly Process . . . . .	33
3.5	Numerical Modelling and Finite Element Analysis . . . . .	38
3.5.1	Mechanical Properties of the Materials . . . . .	39
3.5.2	Contact and Boundary Conditions . . . . .	40
3.5.3	Load Conditions . . . . .	42
3.5.4	FE Mesh Generation . . . . .	44
<b>4</b>	<b>Results and Discussion</b>	<b>49</b>
4.1	FE Knee Joint Models . . . . .	49
4.1.1	Analysis of the Stress-Shielding Effect . . . . .	49
4.1.2	Analysis of the Von Mises Stress Distribution . . . . .	50
4.2	Nodal Analysis of the FE models . . . . .	52
4.3	Influence of changes in the Trabecular Bone Stiffness on the Nodal Von Mises Stress Values . . . . .	56
4.3.1	Trabecular Bone with Young's Modulus of 3GPa . . . . .	57
4.3.2	Trabecular Bone with Young's Modulus of 17GPa . . . . .	58
<b>5</b>	<b>Conclusions</b>	<b>61</b>
5.1	Main conclusions . . . . .	61
5.2	Short-comings, Improvements and Future Work . . . . .	62
	<b>Bibliography</b>	<b>65</b>

# List of Tables

3.1	Material type and the corresponding properties and parameters (Young's Modulus and Poisson's Ratio, attributed to the final FE model of the knee joint, prosthetic components and stems). . . . .	41
3.2	Interactions and constraints applied to the FE models with insertion of the primary prosthesis components and, when applicable, of stems. Indication of the friction coefficient values when applicable. . . . .	42
3.3	Description of the FE models of the knee joint ligaments, including their cross-section area, the interaction between their insertion points and the bones, and their influence radius. . . . .	42
3.4	Orientation of the muscle tendons [Aalbersberg et al., 2005]. . . . .	43
3.5	Ratio to body weight values for the six time instances of the walking gait [Adouni et al., 2012]. . . . .	44
3.6	Muscle tendon forces and reaction forces for each of the six instances of the walking gait.	45
3.7	Element size and element type used for the FE mesh applied on the numerical models of the knee bones and prosthetic components under study. . . . .	46
3.8	Number of nodes and elements of the FE mesh generated on the numerical models of the knee bones. . . . .	46
3.9	Number of nodes and elements of the FE mesh generated on the numerical models of the knee prosthetic components, including both femoral and tibial stems. . . . .	47
4.1	Characterization of the four models analyzed and compared in this study. . . . .	50
4.2	Von Mises stress values of four nodes of the femur surface, for each of the models (Reference, Tibial Stem, Femoral Stem and Both Stems). . . . .	56
4.3	Average Von Mises stress values between the four reference points, for each stance phase percentage, of each model. Relative Deviation between the average Von Mises stress values calculated for the Both Stems model, and the Reference and Tibial Stem models. . . . .	57
4.4	Average Von Mises stress values of all walking gait instances considered, for each reference point. Relative Deviation between the average Von Mises stress values calculated for the Both Stems model, and the Reference and Tibial Stem models. . . . .	57

4.5	Trabecular bone stiffness at 3GPa - Average Von Mises stress values between the four reference points, for each stance phase percentage, of each model. Relative Deviation between the average Von Mises stress values calculated for the Both Stems model, and the Reference and Tibial Stem models. . . . .	58
4.6	Trabecular bone stiffness at 3GPa - Average Von Mises stress values of all walking gait instances considered, for each reference point. Relative Deviation between the average Von Mises stress values calculated for the Both Stems model, and the Reference and Tibial Stem models. . . . .	58
4.7	Trabecular bone stiffness at 17GPa - Average Von Mises stress values between the four reference points, for each stance phase percentage, of each model. Relative Deviation between the average Von Mises stress values calculated for the Both Stems model, and the Reference and Tibial Stem models. . . . .	59
4.8	Trabecular bone stiffness at 17GPa - Average Von Mises stress values of all walking gait instances considered, for each reference point. Relative Deviation between the average Von Mises stress values calculated for the Both Stems model, and the Reference and Tibial Stem models. . . . .	59

# List of Figures

2.1	Knee Joint Representation . . . . .	5
2.2	Anatomical reference planes [Graaff, 2001] . . . . .	7
2.3	Directional terms used for anatomical description in the anatomical position [Van Putte et al., 2016] . . . . .	7
2.4	Frontal view of a typical synovial joint [Derrickson and Tortora, 2017] (a) and Knee joint, an example of a synovial joint, shown in a sagittal view [Graaff, 2001] (b). . . . .	8
2.5	Anterior (left) and Posterior (right) view of a right femur [Graaff, 2001] . . . . .	9
2.6	Anterior (left) and Posterior (right) view of a right tibia, fibula and patella [Graaff, 2001] . .	10
2.7	Anterior (a) and posterior (b) deep view of the right knee joint [Derrickson and Tortora, 2017] . . . . .	11
2.8	Anterior deep view of the right knee joint [Van Putte et al., 2016] . . . . .	12
2.9	Posterior deep view of the right knee joint [Van Putte et al., 2016] . . . . .	12
2.10	Representation of a superior view of the right tibial proximal surface, with the menisci [Derrickson and Tortora, 2017] . . . . .	13
2.11	Representation of the femoral and tibial mechanical and anatomical axes [Kattimani, 2018]	14
2.12	Normal (a), varus (b) and valgus (c) alignment of the knee joint [Completo, 2006]. . . . .	15
2.13	Six degrees of freedom of movement of the knee joint [Hasemkamp, 2013] . . . . .	16
2.14	Rollback mechanism of the femur, combining rotation and gliding movements, over a fixed tibia during (a) flexion and (b) extension [Ganvir et al., 2013] . . . . .	17
2.15	Representation of an osteoarthritic knee, before and after a total knee arthroplasty [Completo, 2006]. . . . .	18
2.16	SIGMA <sup>®</sup> Posterior Stabilized Fixed Bearing Knee Prosthetic [DePuy, 2012] (a) and respective components used in primary surgery: Femoral Component, Tibial Polyethylene Insert and Tibial Tray, from left to right [DePuy, 2010] (b). . . . .	20
2.17	Midline skin incision (a), medial parapatellar incision (b) and osteophyte removal (c). [DePuy, 2014] . . . . .	23
2.18	Proximal tibial resection (a), distal femoral resection (b) and extension gap assessment (c). [DePuy, 2014] . . . . .	23
2.19	Anterior and posterior (a), chamfer (b) and notch (c) femoral cuts. [DePuy, 2014] . . . . .	24

2.20 Exposure of the extensor mechanism (a) following the medial patellar incision and patellar eversion, Disruption of the bone/cement or bone/prosthesis interface (b) before attempted extraction [DePuy, 2013]. . . . .	26
2.21 Extension gap (a) and Flexion gap (b) of the Revision TKA [DePuy, 2013]. . . . .	27
3.1 Topogram and VRT (Volume Rendering Technique) CT image of the female left knee joint CT images. . . . .	30
3.2 Definition of the 3D region of interest for segmentation on ITK-SNAP. . . . .	31
3.3 ITK-SNAP Active contour segmentation mode definition of threshold values. . . . .	31
3.4 ITK-SNAP Active contour segmentation mode placement of the spherical surfaces. . . . .	31
3.5 ITK-SNAP Iterations of contour evolution of the semi automatic segmentation mode, (a) before initiation, (b) after 60 iterations, (c) after 200 iterations and (d) after contour is complete. . . . .	32
3.6 Final ITK-SNAP segmentation model of (a) the left tibia and femur and (b) left fibula. . . . .	32
3.7 3D knee joint model before and after applying Laplacian Smooth Filter, with 4 smoothing steps. . . . .	33
3.8 Original Mesh obtained with the ScanTo3D toolbox in SolidWorks®. . . . .	33
3.9 Computational 3D Solid Model of the knee joint using the SolidWorks® Loft Surface Tool, based on the original mesh obtained with the ScanTo 3D® toolbox. . . . .	34
3.10 Frontal view of the Computational 3D Solid Model of the fibula using the SolidWorks® Loft Surface Tool, based on the original mesh obtained with the ScanTo3D® toolbox. . . . .	35
3.11 Computational 3D models of the (a) Femoral Component, (b) Tibial Insert and (c) Tibial Tray of the SIGMA® PS Fixed Bearing knee prosthesis [Moreira, 2018]. . . . .	35
3.12 Computational 3D models of the (a) Femoral and (b) Tibial Stems and of the modified (c) Femoral and (d) Tibial stems, used for the creation of the intermedullary canals [Moreira, 2018]. . . . .	36
3.13 View of the fully filled bone models and the trabecular bone models displayed on SolidWorks®. . . . .	37
3.14 Anterior (a), Lateral (b), Medial (c) and Posterior views of the 3D computational model of the knee joint with insertion of the SIGMA® Fixed Bearing knee prosthesis, Cortical and trabecular bone displayed on SolidWorks®. . . . .	38
3.15 Insertion points of the (a) MCL, (b) LCL and (c) PTL ligaments, in the FE model. . . . .	40
3.16 Coupling interactions between the prosthetic surfaces and the springs. . . . .	41
3.17 Anterior (a) and Posterior (b) views of the muscle tendon insertion sites. . . . .	43
3.18 Reference point on the femoral surface where reaction forces are applied, reference point on the center of the tibial component where reaction forces are initially measured. Coordinate system used for all forces. . . . .	44
3.19 Mesh applied to the final FE knee joint model. . . . .	46
4.1 Von Mises Stress Distribution (in MPa) for Axial Cuts of the Reference Model femur, at 75% stance phase. . . . .	51

4.2	Von Mises Stress Distribution (in MPa) for Axial Cuts of the Both Stems Model femur, at 75% stance phase. . . . .	51
4.3	0% Stance Phase - Comparison of the femoral Von Mises stress distribution of the Reference, Tibial Stem, Femoral Stem and Both Stems models. . . . .	52
4.4	5% Stance Phase - Comparison of the femoral Von Mises stress distribution of the Reference, Tibial Stem, Femoral Stem and Both Stems models. . . . .	52
4.5	25% Stance Phase - Comparison of the femoral Von Mises stress distribution of the Reference, Tibial Stem, Femoral Stem and Both Stems models. . . . .	53
4.6	50% Stance Phase - Comparison of the femoral Von Mises stress distribution of the Reference, Tibial Stem, Femoral Stem and Both Stems models. . . . .	53
4.7	75% Stance Phase - Comparison of the femoral Von Mises stress distribution of the Reference, Tibial Stem, Femoral Stem and Both Stems models. . . . .	54
4.8	100% Stance Phase - Comparison of the femoral Von Mises stress distribution of the Reference, Tibial Stem, Femoral Stem and Both Stems models. . . . .	54
4.9	Highlighted representation (red dots) of the femoral surface nodes (1 to 4) chosen for analysis. . . . .	55

# Nomenclature

$\epsilon$	Deformation
$\nu$	Poisson's Ratio
$\sigma$	Stress
$\sigma_{bs}$	Stress of the Both Stems Model
$\sigma_r$	Stress of the Reference Model
$\sigma_{ts}$	Stress of the Tibial Stem Model
$E$	Young's modulus
$k_{nn}$	Stiffness in the normal direction
$k_{ss}$	Stiffness in the tangential direction in the 1 element coordinate direction
$k_{tt}$	Stiffness in the tangential direction in the 2 element coordinate direction
$k$	Spring Stiffness
$M_x$	Moment about the x axis at the coordinate system centered at the tibial component
$M_y$	Moment about the y axis at the coordinate system centered at the tibial component
$M_z$	Moment about the z axis at the coordinate system centered at the tibial component
$M'_x$	Moment about the x axis at the coordinate system centered at the femoral surface
$M'_y$	Moment about the y axis at the coordinate system centered at the femoral surface
$M'_z$	Moment about the z axis at the coordinate system centered at the femoral surface

# Acronyms

<b>3D</b>	Three Dimensional.
<b>ACL</b>	Anterior Cruciate Ligament.
<b>BF</b>	Bicep Femoris.
<b>CAD</b>	Computer Assisted Design.
<b>CT</b>	Computed Tomography.
<b>DICOM</b>	Digital Imaging in Medicine and Communications.
<b>FE</b>	Finite Element.
<b>FEA</b>	Finite Element Analysis.
<b>FEM</b>	Finite Element Method.
<b>HU</b>	Hounsfield Unit.
<b>IM</b>	Intramedullary.
<b>LCL</b>	Lateral Collateral Ligament.
<b>MCL</b>	Medial Collateral Ligament.
<b>MRI</b>	Magnetic Resonance Imaging.
<b>OA</b>	Osteoarthritis.
<b>PCL</b>	Posterior Cruciate Ligament.
<b>PMMA</b>	Polymethylmethacrylate.
<b>PS</b>	Posterior Stabilized.
<b>PT</b>	Patellar Tendon.
<b>PTL</b>	Proximal Tibiofibular Ligament.
<b>SM</b>	Semimembranosus.
<b>Ti</b>	Titanium.
<b>TKA</b>	Total Knee Arthroplasty.
<b>TKR</b>	Total Knee Replacement.



# Chapter 1

## Introduction

In this introductory chapter, the subject matter behind the development of this work is presented. Furthermore, the main questions this work will address and the methodology chosen for that purpose are succinctly mentioned.

### 1.1 Motivation and Goals

Over the past half century, the total knee arthroplasty (TKA) has evolved into one of the most successful surgical procedures in modern medicine. The knee is the largest and most complex joint in the human body, and can often be subjected to great amounts of stress during physical activities, such as running or jumping. In addition, knee condition can also deteriorate with age. Osteoarthritis, a disease characterized by the deterioration of cartilage over time due to prolonged wear, is one of the most common chronic conditions affecting adults today. Knee osteoarthritis causes a great deal of pain to the patient, as well as directly decreasing their quality of life. When the deterioration is too severe, TKA is performed so that proper knee joint function is restored, making osteoarthritis the main indication for the procedure. Over the last decades, the number of patients undergoing TKA has considerably and consistently increased. In the United States alone, the number of TKAs performed each year increased from 31.2 per 100 000 person-years between 1971 and 1976, to 220.9 per 100000 person-years between 2005 and 2008 [Eidel et al., 2020]. In 2012 alone, more than 700000 TKAs were performed in the US, with a projected 143% increase in TKA volume by the year 2050 [Inacio et al., 2017]. Not only has TKA proven to be successful in restoring knee functionality, it also provides satisfactory long-term results. In 2010, the survival rate at 10 years for primary TKA was 92% [Putman et al., 2018]. Nevertheless, no surgical procedure is without the possibility of postoperative complications. In the case of TKA, infection and loosening of the prosthetic components are the most common sources of implant failure. Postoperative complications, along with the finite lifespan of 10 to 15 years of the implants, the increasing number of primary TKAs and the expanding indication of the procedure to younger patients, are all collectively responsible for an increased number of revision TKA procedures being performed.

In revision TKA, prosthetic components are removed and replaced, with the goal of reinstating the

desired stability and functionality of the knee joint. Revision TKA must deal with bone loss, inflammatory processes and stress shielding effects, as a consequence of the initial surgical intervention. Furthermore, femoral and tibial components used for primary TKA may no longer provide necessary stability, on their own. As a result, revision TKA may require the use of revision specific components, such as stems, as a complement to the primary components. Stems improve the mechanical stability of the components, by providing load transmission to diaphyseal cortical bone and away from implant interfaces [Shannon et al., 2003], at the cost of stress shielding along their length. This may result in decreased bone density and higher risks of loosening and fracture, hindering long-term implant fixation. However, in revision surgeries where bone loss and instability is already present, increased stability provided by stems is desired [Scott and Biant, 2012]. Undeniably, revision TKA results are promising, with over 70% success rates at 3.5 years. However, these are still inferior to the results of primary TKA, due to the complicated nature of the procedure and the restrictions caused by bone loss, as previously mentioned [Completo, 2006].

Modern imaging methods and CAD-software allow the reconstruction and design of biological structures, suitable for computational finite element analysis (FEA). FEA is used to solve biomechanical problems involving the study of tissues, such as bones, as well as their mechanical behaviour, under different conditions [Klues, 2010]. In particular, joint replacement surgeries can be assessed pre-operatively, making the procedure more personalized to the specific needs of each patient. This way, the outcome of surgical procedures can be improved. In that sense, the main goal of this study is to understand how the introduction of an intermedullary stem, during revision TKA, affects the stresses acting on the complementary bone. Four different computational models for FEA were created, representing the knee joint after primary surgery, without any stem, and three possible knee joint configurations after revision surgery, with the insertion of only a femoral or a tibial stem, or both. Comparing the four, the goal is to determine if, indeed, one stem influences the stresses on the complementary bone.

## 1.2 Thesis Outline

In order to present all the information in a cohesive and organized manner, this work has been divided into five main chapters. Firstly, the subject matter of this study is introduced, as well as concepts considered relevant to its full comprehension. Following that, the methodology used for the analysis performed is described. Finally, the obtained results and main conclusions are presented, as well as suggestions for future works. Starting with chapter 1, the subject that led to this work is introduced, and the main motivations and goals are presented.

Ensuing, in Chapter 2, an introduction to the main topics concerning the comprehension of the developed study is provided. This information includes an initial description of the knee joint anatomy and biomechanics. Then, the total knee arthroplasty is described, including the possible indications and contraindications for this kind of surgery, as well as the complications that can occur. Furthermore, the type of prosthesis used for this particular study is also described, as well as the technique used in these surgeries. Revision surgery is also mentioned, as a result of the possible complications. In this case,

the surgical technique is also described.

In chapter 3, the methodology used to achieve the numerical models is described. Initially, the image acquisition and segmentation process is described, followed by the computational modelling of the 3D knee joint models, with resource to CAD software. Finally, the models created are used to obtain the numerical models with which the finite element analysis is performed. All implementation decisions made for the numerical models, including the mechanical properties, the contact and boundary conditions, the load conditions and mesh generation, are thoroughly explained. In chapter 4, the results obtained are stated and analyzed. In chapter 5, the main conclusions drawn from the study and possible future improvements are presented.



## Chapter 2

# Background

The information presented in this chapter is intended to provide insight on the theoretical basis behind the work developed in this study. Firstly, a thorough introduction to the knee joint anatomy is provided. Furthermore, as the proper functioning of prosthetic joint components heavily relies on the understanding of joint kinematics, relevant concepts of knee alignment and knee biomechanics are also explained. Ensuing, an overview of the total knee arthroplasty is also provided, including possible indications for surgery, as well as complications that may occur. Epidemiological data on TKA is also mentioned. Additionally, the prosthesis chosen for this study and accompanying surgical techniques are also described, for both primary and revision surgeries. Finally, revision total knee arthroplasty is also mentioned, as the inclusion of stems in TKA is to be studied and discussed in future chapters.

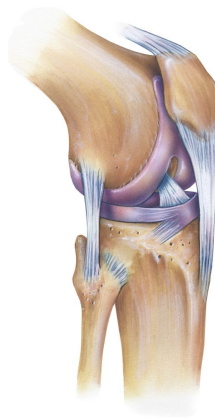


Figure 2.1: Knee Joint Representation

### 2.1 Knee Joint

The knee joint (Figure 2.1) is the largest and most complex joint in the human body. It is comprised of two distinct joints: the tibio-femoral joint and the patella-femoral joint. The tibio-femoral joint refers to the joint formed by the proximal tibia and the distal femur. It is responsible for flexion and extension movements of the leg, crucial for activities such as walking or running. The patella-femoral joint,

formed by the patella and femur, stabilizes and protects the knee joint, with the former gliding over the latter. In addition, various stabilizers act simultaneously, in order for the knee joint to move correctly and with proper stability. The stabilization is guaranteed, primarily, by the ligaments located around the knee, while secondary stabilization is provided by the surrounding muscles. In addition, the menisci, two fibro-cartilaginous discs located above each tibial condyle, act as shock absorbers. These are responsible for providing protection and increasing the stability of the knee [Affatato, 2015, Abulhasan and Grey, 2017].

The knee joint can tolerate considerable stress without damage. Nonetheless, when subjected to sudden forceful stresses, injuries can occur. As a result, surgery may be necessary [Graaff, 2001]. Furthermore, poor knee alignments damage the articulation, and may also be corrected through surgical intervention. Knee interventions are complex procedures, and the lack of vascularity of the cartilaginous tissue difficults healing. Thus, knowledge of the knee's anatomy and biomechanics is important for medical professionals, as it provides insight regarding the joint's limitations [Graaff, 2001]. The knee joint and its anatomical components will be further described in the following subsections.

### **2.1.1 Descriptive Terminology**

When referring to anatomical structures, it is standard practice to use precise relational terminology. As this terminology will be used extensively throughout this work, it is relevant to briefly summarize the directional terms used when referring to the different anatomical structures that comprise the knee joint. These are all relative to the anatomical reference position, in which the person stands erect looking forward. The upper limbs hang to the sides, with palms facing forward and thumbs facing away from the body, while the feet are parallel to each other, facing forward and flat on the floor [Van Putte et al., 2016].

Three main anatomical planes section the human body, the sagittal, frontal and transverse planes, shown in Figure 2.2. The sagittal or longitudinal plane divides the body into left and right halves; the frontal or coronal plane divides the body in anterior and posterior halves; while the transverse or horizontal plane divides it into superior and inferior halves. Additionally, three anatomical axes exist, around which the body or body parts can rotate. These are perpendicular to each other and to the anatomical planes already mentioned. There is the transverse axis, perpendicular to the sagittal plane; the sagittal or anteroposterior axis, perpendicular to the frontal plane; and finally, the longitudinal axis, perpendicular to the axial plane.

The directional terms used to describe the halves divided by each plane can also be used to describe anatomical structures, as shown in Figure 2.3. Furthermore, the terms medial and lateral are used to describe the proximity to the body's midline. For example, at the knee joint level, each distal femoral end is divided into two condyles, a medial one, closest to the midline, and a lateral one, which is further away. When referring to the limbs, one can also use the terms proximal and distal. Using the example of the femur once more, the proximal end of the femur is at the hip joint while the distal end is at the knee joint.

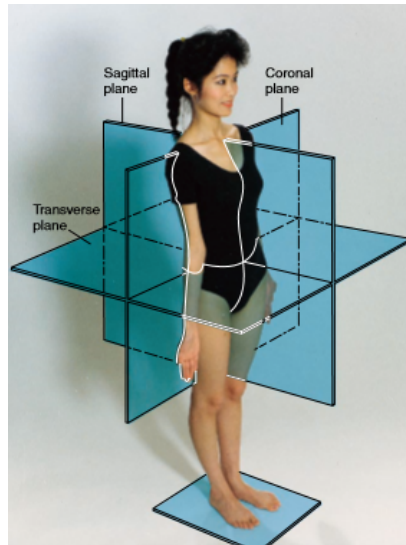


Figure 2.2: Anatomical reference planes [Graaff, 2001]

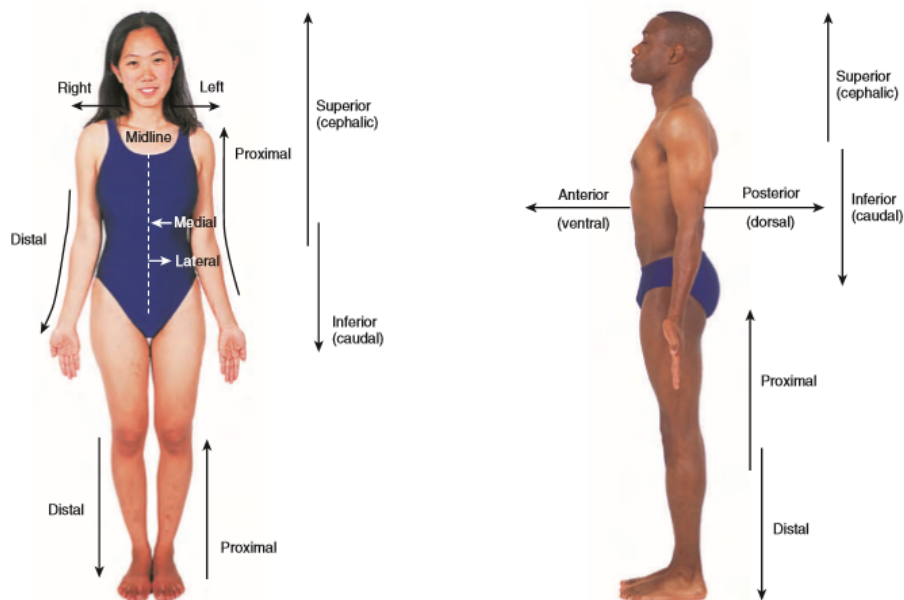


Figure 2.3: Directional terms used for anatomical description in the anatomical position [Van Putte et al., 2016]

## 2.1.2 Synovial Joint

A joint, or articulation, is a junction of two bones, which can exhibit different ranges of motion. While many move in a limited manner, others are almost, or completely, immovable. Thus, the degree of movement allows the joint to be classified, functionally, as a synarthrosis (non-movable), an amphiarthrosis (slightly movable) or a diarthrosis (freely movable) [Van Putte et al., 2016]. Joints can also be classified structurally, according to the type of connective tissue that binds the bones together and whether it is surrounded by a fluid-filled joint capsule. The three major structural classes of joints are fibrous, cartilaginous, and synovial [Van Putte et al., 2016].

The knee is classified as a synovial joint (Figure 2.4(a)), as it contains an articular capsule, which

encloses the joint bones. Inside the capsule is the joint cavity, filled with synovial fluid. This fluid, responsible for the lubrication of the joint, is rich in hyaluronic acid and is secreted by a thin synovial membrane that lines the inside of the joint capsule [Graaff, 2001]. The articular surfaces of the bones comprising the synovial joint are covered with a smooth layer of hyaline cartilage, called the articular cartilage. In addition to the internal synovial membrane, the capsule is covered externally with a fibrous membrane, which in certain parts thickens to form ligaments that support the joint. In certain synovial joints, such as the knee, small sacs lined with synovial membrane and filled with fluid can be found in locations where friction might occur. A structure of this nature is called a bursa, and is responsible for cushioning the contact between certain muscles or tendons over bones or ligaments [Graaff, 2001]. As for the knee joint, in particular, pads of fibrocartilage called menisci are also present, in order to cushion the contact between femoral and tibial articular surfaces (Figure 2.4(b)).

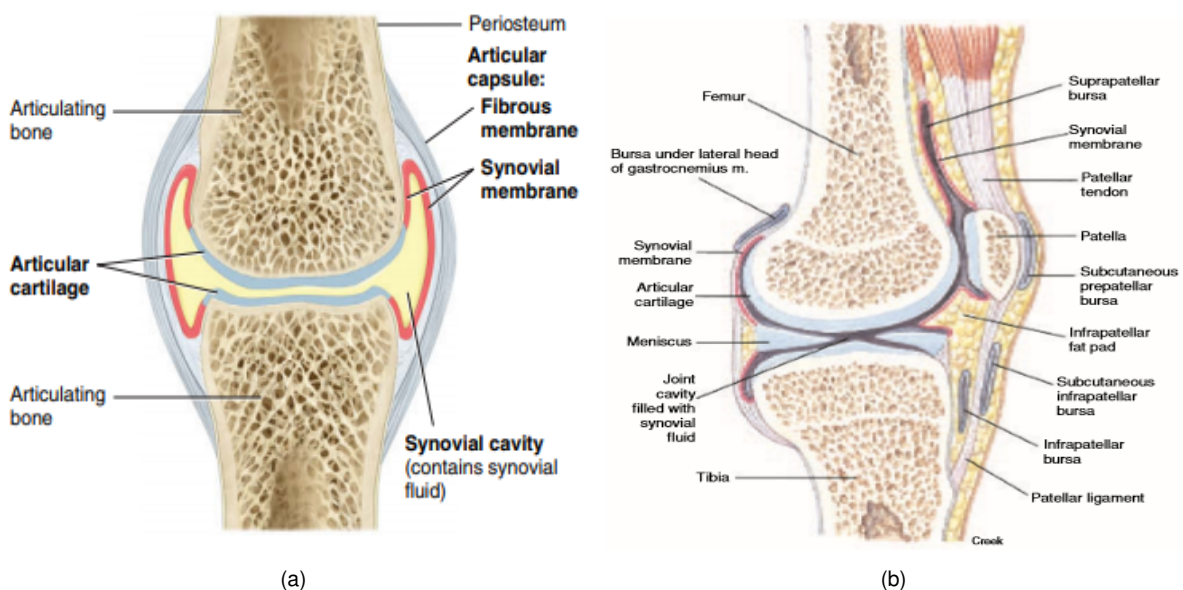


Figure 2.4: Frontal view of a typical synovial joint [Derrickson and Tortora, 2017] (a) and Knee joint, an example of a synovial joint, shown in a sagittal view [Graaff, 2001] (b).

Synovial joints are the most freely movable type of joints. Most of the joints in the appendicular skeleton are classified as synovial joints, providing the limbs with great mobility compared to the axial skeleton [Van Putte et al., 2016]. The synovial joint can be classified on the shape of the articulating surfaces. The knee, in particular, is classified as a hinge joint, since movement is allowed, for the most part, in one plane only. The articulation between the femoral and tibial condyles allows flexion and extension, with limited rotation and gliding.

### 2.1.3 Knee Joint Anatomy

As previously mentioned, the knee is a complex joint which requires various anatomical structures to function with proper mobility without sacrificing stability. In the following subsections, these structures, including bones, muscles, ligaments, tendons and menisci are described in detail.

### 2.1.3.1 Femur

The femur, represented in Figure 2.5, is the longest and heaviest bone in the human body. As a long bone, it is comprised of two epiphyses and a diaphysis. The femoral head is located at the proximal epiphysis, which articulates with the pelvic acetabulum to form the hip joint. Moving distally, the diaphysis is slightly curved anteriorly and medially. On its posterior surface, a roughened vertical ridge where several muscle insertions occur, called linea aspera, is present [Graaff, 2001]. The distal epiphysis is divided into two condyles, which in conjunction with the proximal end of the tibia, form the tibio-femoral joint.

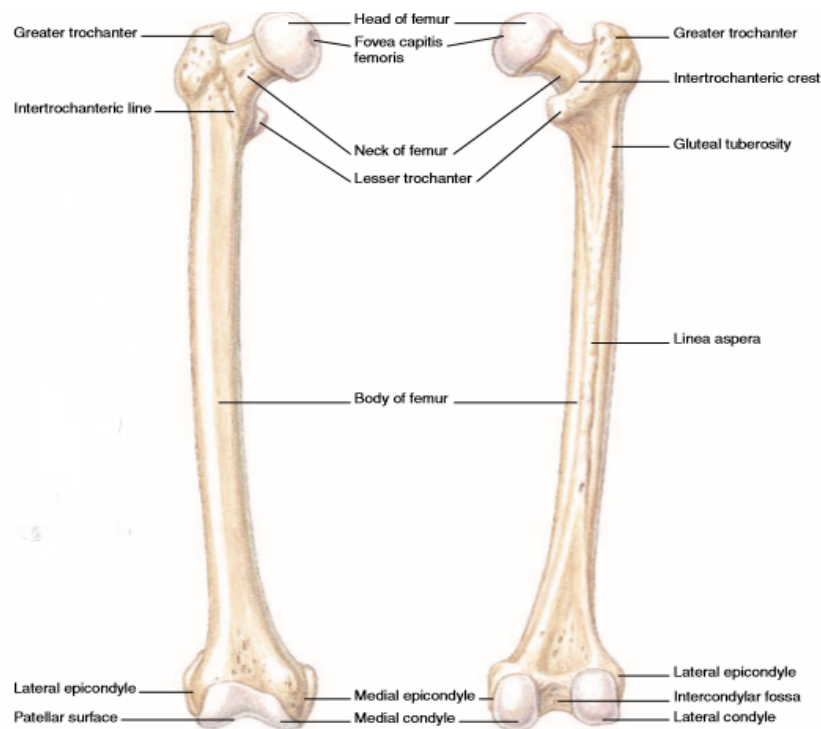


Figure 2.5: Anterior (left) and Posterior (right) view of a right femur [Graaff, 2001]

The femoral condyles are two oblong and convex prominences covered by smooth hyaline cartilage [Affatato, 2015]. The two are separated posteriorly by a depression, the intercondylar fossa. Anteriorly, the patellar surface can be found, where the patella glides over during knee flexion and extension. The two condyles are shaped differently, with the lateral being flatter and larger. It is also more in line with the femoral shaft, resulting in more weight transmission to the tibia [Affatato, 2015]. The medial condyle is narrower, with a larger rolling surface. The epicondyles are located right above the condyles, acting as attachment points for ligaments and tendons. In this particular case, the collateral ligaments attach to the femur at the epicondyles.

### 2.1.3.2 Tibia and Fibula

The tibia, represented in Figure 2.6, is located in the lower leg, medial to the fibula. A long bone, much like the femur, it is comprised of a diaphysis and two epiphyses. The diaphysis decreases in volume distally [Affatato, 2015]. The proximal epiphysis expands transversally and is divided into two

slightly concave condyles which articulate with the corresponding convex condyles of the femur. On the upper surface of the tibial condyles, a layer of hyaline cartilage is found, as well as a tibial eminence, separating the medial and lateral condyles. This bony projection is an attachment point for the cruciate ligaments, as well. The tibial tuberosity is located on the proximoanterior part of the tibial body, serving as the attachment point of the patellar ligament [Graaff, 2001]. Moving distally, a sharp ridge runs along the tibial shaft, known as anterior border or shin. Distally, on the medial side, a prominence called the medial malleolus is found, which articulates with the talus bone to form the ankle joint. On the distolateral side, the fibular notch articulates with the fibula.

The fibula, shown as well in Figure 2.6, is lateral to the tibia and both are connected by an interosseous membrane. In addition to the distal articulation, the fibular head articulates proximally with the tibia, at the inferior surface of the lateral tibial condyle. The fibula, similarly to the tibia, presents a distal projection, the lateral malleolus, which articulates with the talus bone, at the ankle joint.

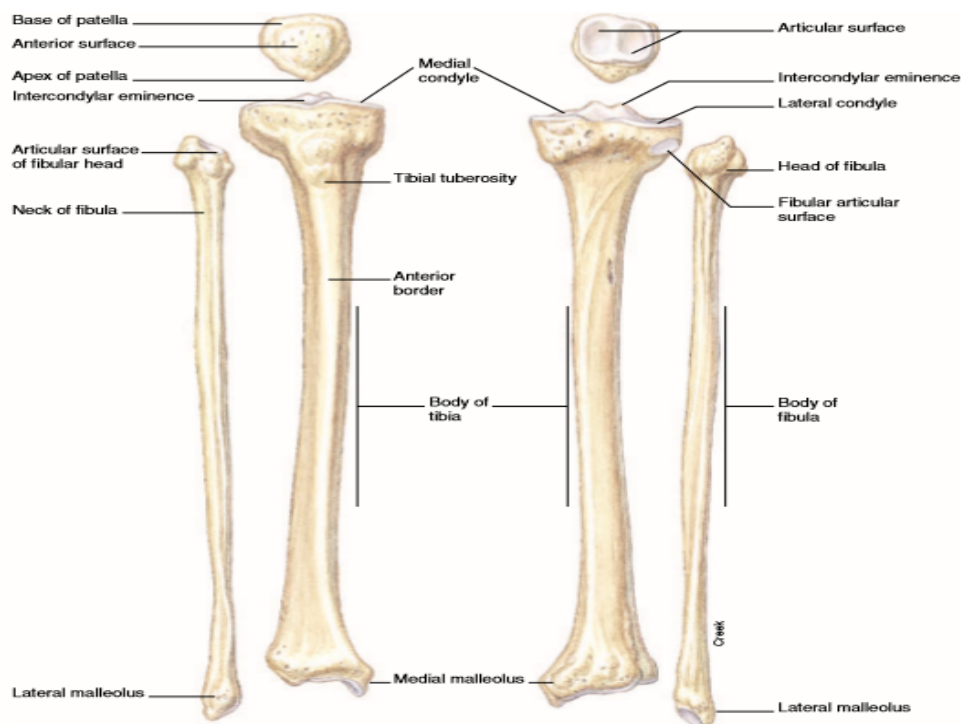


Figure 2.6: Anterior (left) and Posterior (right) view of a right tibia, fibula and patella [Graaff, 2001]

### 2.1.3.3 Patella

The patella (Figure 2.6) is the largest sesamoid bone in the human body, located anterior to the distal femur and embedded in the quadriceps tendon [Affatato, 2015]. It is a flat, curved bone, with the exception of its triangularly shaped distal end. This distal apex attaches to the patellar ligament portion of the quadriceps tendon, connecting the patella to the tibial anterior tuberosity. The patella has both anterior and posterior surfaces, the latter articulates with the femur. Functionally, the patella protects the knee joint, while also increasing the leverage of the quadriceps femoris muscle [Graaff, 2001].

#### 2.1.3.4 Ligaments, Muscles and Tendons

Ligaments are fibrous bands of connective tissue that connect bones together and provide support to joints, acting as their main stabilizers [Abulhasan and Grey, 2017]. As many synovial joints, the knee's articular capsule is surrounded by external ligaments. Furthermore, the knee is also stabilized by a pair of intracapsular ligaments, the cruciate ligaments. Regarding the extracapsular ligaments, the knee joint is surrounded by five different ligaments, the collateral ligaments, lateral and medial, the patellar ligament, the oblique popliteal ligament and the arcuate popliteal ligament. The lateral (or fibular) collateral ligament (LCL) is a rounded ligament that attaches to the lateral femoral epicondyle and extends to the lateral side of the fibular head. It prevents lateral displacement, or varus stress, of the knee. The medial (or tibial) collateral ligament (MCL) is flat and broad in shape, attaches to the medial femoral epicondyle and extends to the medial tibial surface, below the medial condyle. The MCL is responsible for preventing medial displacement, or valgus stress, of the knee. Both collateral ligaments are represented in Figure 2.7. On the anterior surface is the patellar ligament, which is the portion of the quadriceps tendon that extends from the patellar apex to the tibial tuberosity, stabilizing the patella. The posterior surface of the knee joint is stabilized by the oblique popliteal ligament, from the intercondylar fossa and lateral femoral condyle to the medial condyle of the tibia, and the arcuate popliteal ligament, from the lateral femoral condyle to the fibular head, as represented in Figure 2.7(b) [Derrickson and Tortora, 2017].

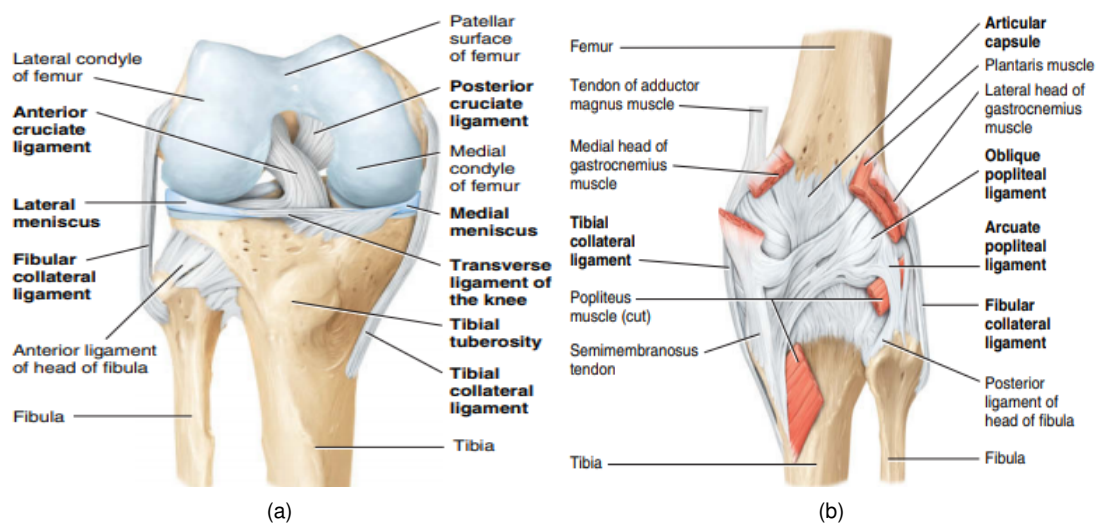


Figure 2.7: Anterior (a) and posterior (b) deep view of the right knee joint [Derrickson and Tortora, 2017]

The anterior and posterior cruciate ligaments are two intracapsular ligaments, responsible for connecting the femur and the tibia together. As previously mentioned, these ligaments attach distally at the tibial eminence, crossing each other, as shown in Figure 2.7(a). The anterior cruciate ligament (ACL), attaches to the tibia anteriorly, immediately behind the medial meniscus, and extends laterally to attach to the posteromedial side of the femoral lateral condyle. It is responsible for limiting hyperextension of the knee, while simultaneously preventing the anterior sliding of the tibia over the femur (or posterior sliding of the femur over the tibia) [Derrickson and Tortora, 2017]. The posterior cruciate ligament (PCL),

attaches posteriorly to the tibia, crossing over the ACL, and attaching to the anterolateral side of the medial femoral condyle. The PCL also limits hyperextension and prevents posterior sliding of the tibia over the femur (or anterior sliding of the femur over the tibia) [Derrickson and Tortora, 2017].

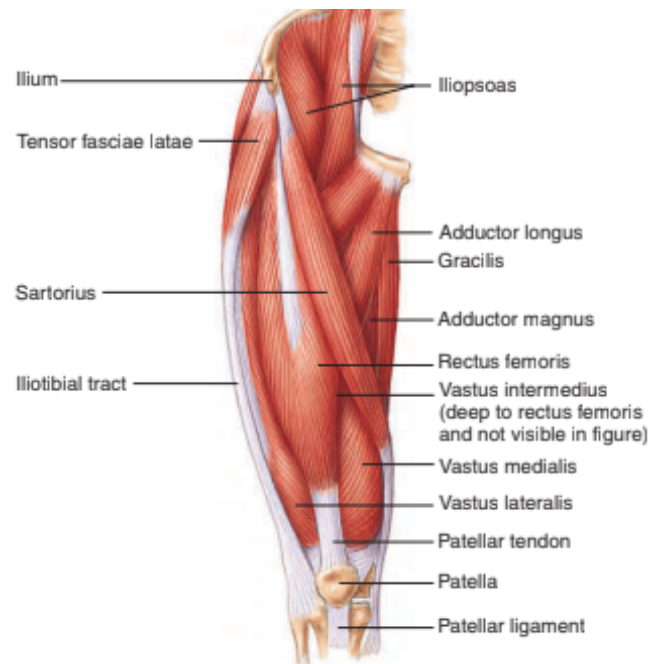


Figure 2.8: Anterior deep view of the right knee joint [Van Putte et al., 2016]

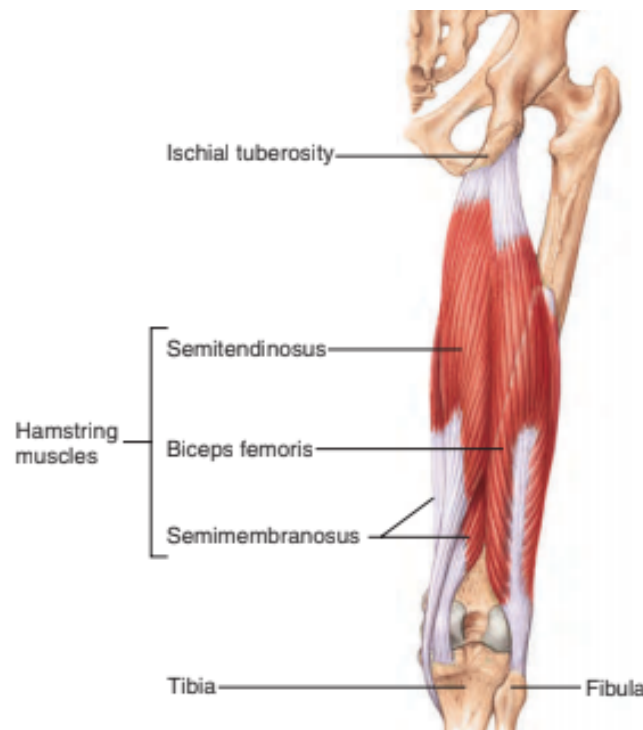


Figure 2.9: Posterior deep view of the right knee joint [Van Putte et al., 2016]

In addition to the ligaments, the muscles surrounding the knee joint also play a role in knee stabilization, complementary to their primary function of mobilizing the knee. As previously mentioned,

the knee is a hinge joint that allows opposing flexion and extension movements in the sagittal plane, as well as rotation and gliding motions. Thus, the muscles acting on the knee can be divided into two groups according to their primary function: the extensors and the flexors. Muscles involved in knee extension (and hip flexion) are found on the anterior side of the knee, and include the sartorius and the quadriceps femoris. The sartorius is the longest muscle in the human body and it crosses the anterior thigh obliquely, originating from the anterior superior iliac spine and inserting at the medial side of the tibial tuberosity. The quadriceps femoris is considered the main extensor of the knee, and is composed of four different muscles: the rectus femoris, the vastus lateralis, the vastus medialis and the vastus intermedius, shown in Figure 2.8. The rectus femoris originates from the ilium, the vastus lateralis originates from the great trochanter and linea aspera of the femur, the vastus medialis originates from the linea aspera of the femur and the vastus intermedius originates from the body of the femur [Van Putte et al., 2016]. All four muscles composing the quadriceps femoris insert in the patella, via the quadriceps tendon. Distal to the patella, the quadriceps tendon extends as the patellar tendon, and inserts in the tibial tuberosity. Antagonistic to these are the hamstring muscles, responsible for knee flexion (and hip extension). These are three different muscles, the bicep femoris, the semimembranosus and the semitendinosus, as shown in Figure 2.9. The bicep femoris is the most laterally placed of the three. It originates from the long head of the ischial tuberosity and inserts at the fibula and lateral tibial epicondyle. Complementary to flexion, it is also responsible for laterally rotating the leg. The semimembranosus originates from the short head of the ischial tuberosity and the semitendinosus originates from the ischial tuberosity. Both insert on the medial tibial surface and are also responsible for internal rotation of the leg [Van Putte et al., 2016].

#### 2.1.3.5 Menisci

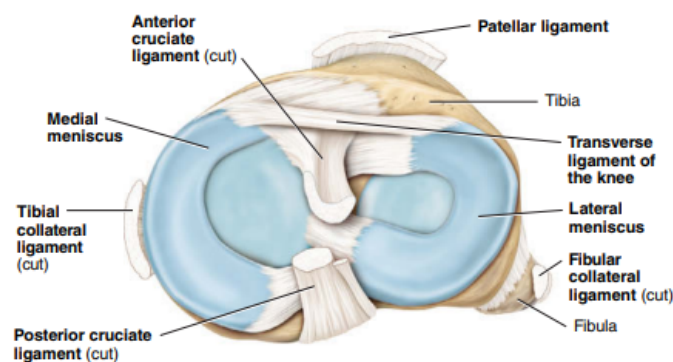


Figure 2.10: Representation of a superior view of the right tibial proximal surface, with the menisci [Derrickson and Tortora, 2017]

Although the femoral and tibial condyles present complementary shapes (convex and concave, respectively), their respective articular surfaces are not congruent. Due to that, fibrocartilaginous pads are located between the condyles. These are the menisci, which assist the articular surfaces during activity. The knee joint presents two menisci, one medial and one lateral, connected to the tibia through the anterior and posterior cruciate ligaments [Affatato, 2015], and to each other through the transverse ligament, as exemplified in Figure 2.10. Each meniscus displays a particular shape, the lateral is nearly

circular, while the medial has a more semicircular form. Mobility also differs, as the lateral meniscus is more mobile than the medial one.

Functionally, these provide a frictionless surface that allows joint movement, in addition to playing a fundamental role in shock absorption [Abulhasan and Grey, 2017]. The menisci allow the distribution of contact stresses over the entire extent of the tibial plateau, which is crucial for the preservation of the articular cartilage, and overall condition of the knee joint.

## 2.2 Knee Alignment

The alignment between the hip, knee and ankle joint is a key factor for load distribution on the knee joint. In order to assess if the knee is properly aligned, two main axes are considered: the mechanical and the anatomical axes. Firstly, as a reference, the vertical axis is drawn vertically from the center of the pubic symphysis, extending distally. The mechanical axis of the lower extremity is determined by drawing a line from the center of the femoral head to the center of the ankle joint. This corresponds to an approximated  $3^\circ$  slope from the vertical axis. One can also divide the mechanical axis into femoral and tibial mechanical axes. The femoral mechanical axis starts at the femoral head and runs distally to the intercondylar notch of the distal femur. The tibial mechanical axis runs from the proximal tibia to the the ankle center, passing just medially to the tibial eminence [Cherian et al., 2014].

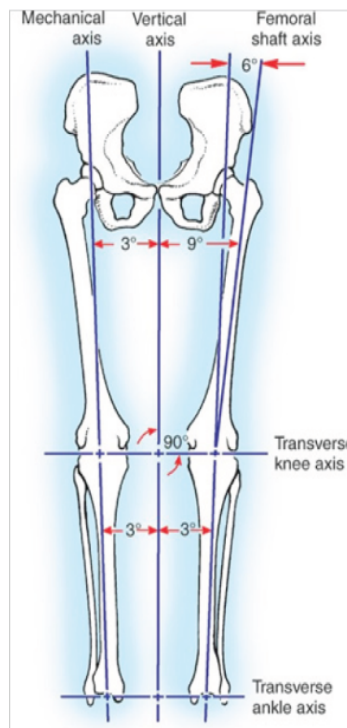


Figure 2.11: Representation of the femoral and tibial mechanical and anatomical axes [Kattimani, 2018]

The anatomical axes, however, are relative to the intermedullary canals. The femoral anatomical axis is determined as a line that bisects the femoral shaft, while the tibial anatomical axis bisects the tibia. From a frontal plane perspective, when comparing the mechanical and anatomical axes, the two tibial axes are coincident. The same can't be said about the femur, where an approximate 5 to

7° difference between the two angles is visible. All the axes mentioned are represented in Figure 2.11.

### 2.2.1 Varus and Valgus Alignments

As already mentioned, the mechanical axis is defined as the line that goes from the center of the hip joint to the center of the ankle joint. Normal alignment of the knee (Figure 2.12(a)) occurs when the mechanical axis runs through the center of the knee [George, 2019]. When this angle is not correct, a deformity occurs, resulting in damage to the articular cartilages. If the mechanical axis passes medial to the knee, a varus deformity occurs, as represented in Figure 2.12(b). This misalignment creates a moment arm which results in increased force around the medial compartment [Sharma et al., 2001]. Contrarily, if the mechanical axis passes lateral to the knee, the knee presents a valgus deformity, shown in Figure 2.12(c). In this case, the moment arm increases force across the lateral component [Sharma et al., 2001]. Either misalignment has repercussions on the loading the knee is subjected to. Consequently, the knee's articular damage and corresponding rate of progression are increased when a misalignment is present. In some cases, total knee arthroplasty is necessary to restore the mechanical axis and soft tissue balance, both crucial to knee joint stability.

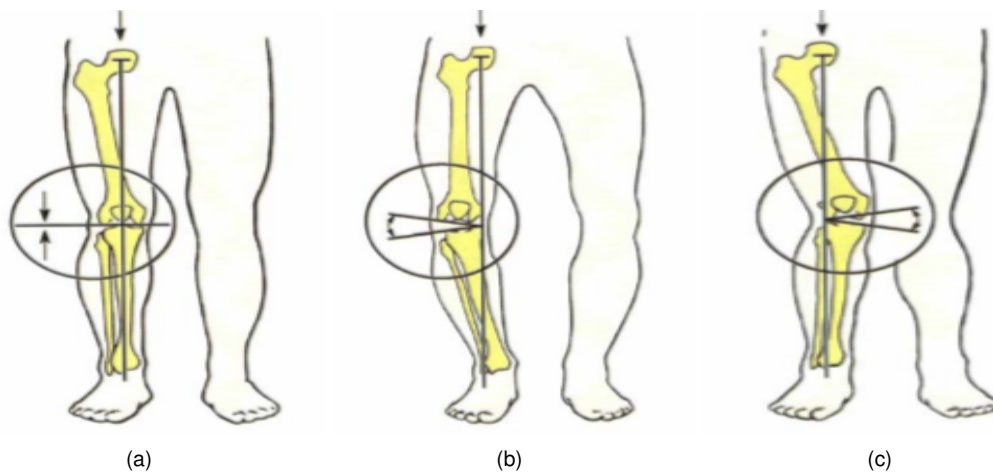


Figure 2.12: Normal (a), varus (b) and valgus (c) alignment of the knee joint [Completo, 2006].

## 2.3 Knee Joint Biomechanics

Mechanics is the field that studies forces and its respective effects. The study of biomechanics applies mechanical concepts to living bodies, in particular to the human locomotor system. Kinematics is the branch of mechanics that analyzes the motion of objects, without taking into account the forces that produce the motion. It differs from kinetics, which concerns the study of the forces acting on a body and its effects in body motion [Bergmann and Peterson, 2011]. Biomechanics also includes statics, the field that studies forces and moments in equilibrium, and dynamics, that studies the body in motion [Affatato, 2015].

The knee is a complex joint, both anatomically and functionally. Thus, knowledge of joint kinemat-

ics is important, as understanding the motion of a healthy knee is crucial for diagnosing certain injuries or pathologies, assessing quantitatively a treatment's effectiveness, as well as improving the development of prosthetic devices [Affatato, 2015].

### 2.3.1 Knee Joint Kinematics

Kinematics describes the motion of multi-link systems, without reference to the causes of motion. Joint kinematics, therefore, studies the motion between two consecutive segments of the human skeleton, by considering them as rigid bodies [Affatato, 2015]. The knee joint, being a mobile joint, presents motion in six degrees of freedom: three rotations and three translations. These movements occur along the three main anatomical planes previously mentioned in Subsection 2.1.1: the sagittal, frontal and transverse planes. Respectively, the translational movements that occur are medial-lateral, anterior-posterior and proximal-distal. Rotational movements that occur on these planes are extension-flexion, varus-valgus and internal-external, respectively (Figure 2.13). Translation movements are significantly restricted by the fibrous capsule, along with the muscles and ligaments surrounding the knee [Affatato, 2015]. Rotation wise, flexion-extension movements show the largest range of motion, while the varus-valgus and internal-external rotations are restricted.

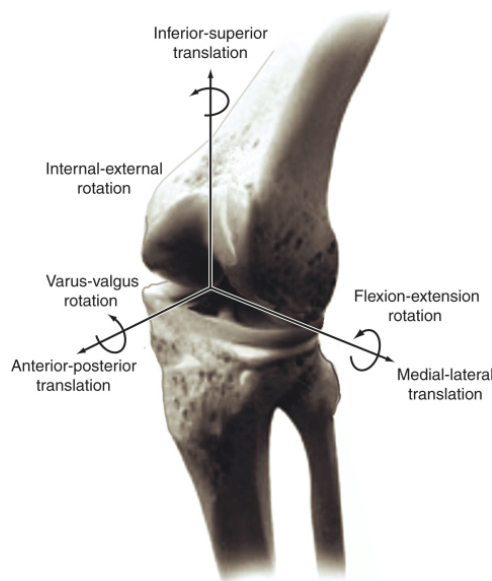


Figure 2.13: Six degrees of freedom of movement of the knee joint [Hasemkamp, 2013]

This results from the hinge nature of the knee joint, which presents flexion-extension as its primary rotational movement, with a range of motion from full extension to full flexion of  $0^\circ$  to  $140^\circ$  [Affatato, 2015]. Complementary to flexion and extension, the knee also allows rolling and gliding of the femoral condyles over the tibial plate during flexion and extension. The combination of all movements, named rollback, is essential to ensure the femur does not run out of the tibia during movement, as a result of articular surface size discrepancies [Ganvir et al., 2013]. Therefore, when flexion occurs, the femoral condyles roll posteriorly (between  $0^\circ$  and  $10^\circ/15^\circ$  flexion), followed by anterior gliding (from  $10^\circ/15^\circ$  to  $140^\circ$  flexion) [Affatato, 2015]. Reversely, in the case of extension, the femoral condyles initially roll

anteriorly, followed by a posterior glide. The cruciate ligaments are intimately connected to the flexion and extension movements. If assumed to be rigid elements with constant length, the ACL can be considered tightened during flexion movements, due to the posterior roll of the femur. This state of the ACL results in an anterior translational force on the femoral condyles. Similarly, during extension the PCL tightens, as a result of the femoral anterior roll. In this case, a posterior translational force acts on the femoral condyles [Ganvir et al., 2013]. The rollback mechanism is represented in Figure 2.14, for the case of a fixed tibia, as when one sits down and gets up, for example. In the case of a fixed femur, the tibial plateau glides and rolls posteriorly during flexion and anteriorly during extension, over the femoral condyles [Ganvir et al., 2013]. The rollback mechanism is considered as the reason for the 140° range of motion shown by the knee joint. Without rollback, impingement of the soft tissues between the posterior femur and the posterior tibia would occur, limiting flexion to between 90° and 105° [Kim et al., 1997].

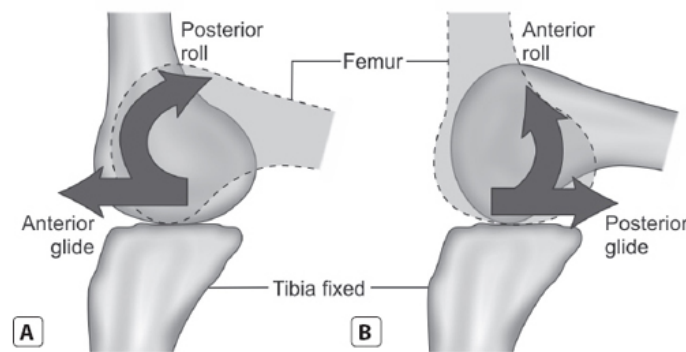


Figure 2.14: Rollback mechanism of the femur, combining rotation and gliding movements, over a fixed tibia during (a) flexion and (b) extension [Ganvir et al., 2013]

The gliding motion is not symmetrical for the femoral condyles, as the two present morphological differences, as previously mentioned. Due to that, gliding occurs firstly on the medial condyle, followed by the lateral condyle [Affatato, 2015]. As for the remaining rotational motions, internal (up to 15° during flexion) and external rotation (up to 30° during flexion) in the transverse plane are automatic, and related to the degree of flexion, due to the 'screwhome' phenomenon [Mansfield and Neumann, 2018]. During flexion, the femoral condyles rotate slightly internally, while full extension is associated with a slight external rotation of the femoral condyles, locking the knee into extension. This locking mechanism can occur by rotation of the tibia on the femur or by rotation of the femur over a fixed tibia [Mansfield and Neumann, 2018]. Additionally, varus and valgus rotation increases with knee flexion, but is very restrained by the surrounding soft tissues, moving only a few degrees [Affatato, 2015].

It is important to mention that the centre of rotation for flexion and extension is not fixed, as a result of the incongruent condylar surface. Instead, the instant centre of rotation moves on a semicircular curve on the condylar plane. This translation of the instant centre of rotation is believed to be controlled by the cruciate ligaments [Affatato, 2015].

## 2.4 Total Knee Arthroplasty

The Total Knee Arthroplasty (TKA) is a surgical procedure involving the substitution of the knee joint by an artificial prosthetic with the goal of restoring knee alignment and reducing pain, therefore improving the patient's quality of life. (Figure 2.15). It is a standard procedure when significant damage and wear to the knee joint is present, and it is currently one of the most successful surgeries in the medical field, with remarkable long-term outcomes [Malizos and Varitimidis, 2017, Tigani et al., 2015].



Figure 2.15: Representation of an osteoarthritic knee, before and after a total knee arthroplasty [Completo, 2006].

In the following subsections, the indications for the surgery, as well as the complications that may occur and consequently lead to revision, are described. Furthermore, the specific prosthesis type used in this study, as well as the surgical techniques for both primary and revision surgeries, are also described in detail.

### 2.4.1 Indications and Contraindications

As previously mentioned, TKA is recommended for cases where the knee joint is severely damaged by diseases such as osteoarthritis or rheumatoid arthritis, or by a traumatic knee injury or deformity. In severe cases, chronic pain is debilitating to the patient, leading to a significant decrease in quality of life. Therefore, the main goal of a TKA is to restore joint stability and relieve pain [Affatato, 2015]. Nevertheless, a knee arthroplasty should only be considered once all other options, such as medication, physical therapy or arthroscopy, for example, have been exhausted [Completo, 2006]. The typical patient that undergoes this type of surgery is usually older, with a more modest lifestyle, as activity levels have an impact on the implant's lifetime. However, the number of TKAs performed every year has been steadily increasing, becoming more and more a reality for an increasing number of younger patients suffering from joint problems and instability. Symptomatology includes limiting and unbearable knee pain, stiffness, instability, swelling and/or varus/valgus deformities. In the majority of cases, such symptoms are consequential of knee pathologies like osteoarthritis and rheumatoid arthritis, as already mentioned [Completo, 2006].

Osteoarthritis is the most common type of arthritis. An age related disease in most cases, it is caused by prolonged wear of the articular cartilage. It leads to inflammation and destruction of the cartilage, until the bones are left in direct contact [Affatato, 2015]. Rheumatoid arthritis is an autoimmune

disease, which can deform the knee joint. It causes inflammation of the synovial membrane surrounding the joint, which becomes thicker and swollen. Synovial liquid production is ceased [Completo, 2006], and the cartilage is progressively destroyed, causing joint pain and stiffness [Affatato, 2015]. Furthermore, in some cases, severe knee injuries can result in post-traumatic arthritis, which may require surgery to substitute the damaged joint.

Still, when active articular infection is present, TKA is not recommended [Completo, 2006]. Furthermore, patients with pre-existing conditions, such as diabetes or uncontrolled hyperglycemia, are at greater risk of infection and postoperative complications. Other risk factors include, previous fractures, obesity, smoking and vigorous high-impact physical activity [Malizos and Varitimidis, 2017].

## **2.4.2 Prosthesis Choice and Posterior Stabilized Fixed Bearing Knee Prosthesis**

Knee prostheses can be classified into three major categories, unconstrained, semiconstrained and constrained. The surgeon chooses which prosthesis to use according to the underlying condition of the patient, the degree of articular damage present and the age of the patient. An unconstrained prosthesis maintains the knee anatomical structure intact, only replacing a small portion or thin layer of the articular surface. A semiconstrained prosthesis, much like the unconstrained, is recommended for superficial replacement of the joint. For this kind of prosthesis, the PCL can often be sacrificed and in such cases, a posterior stabilized implant can be used [Tateishi, 2001]. The use of posterior stabilized design for TKA is becoming increasingly popular as its benefits include easier balancing of varus/valgus deformities and greater posterior femoral rollback. Furthermore, it is possible that it may also result in less component wear and greater flexion range [Indelli et al., 2014]. Finally, constrained prostheses are recommended for greatly damaged and unstable knees, as well as for revision surgeries. In these, the PCL is sacrificed, and the femoral and tibial components are connected by a hinge [Tateishi, 2001].

### **2.4.2.1 Primary TKA**

In this study, the knee prosthesis referenced is the SIGMA<sup>®</sup> Posterior Stabilized (PS) Fixed Bearing Knee System (Figure 2.16(a)). When used in a primary TKA, it is comprised of 3 main components, a femoral component, a tibial tray and a tibial insert (Figure 2.16(b)). In cases where the patellofemoral joint is replaced as well, a patellar component is also included.

Firstly, the SIGMA<sup>®</sup> PS Femoral Component presents a rounded coronal geometry, which allows maximal contact area with minimal contact stresses, for both neutral alignment and varus/valgus lift-off. This design prevents edge loading, which can result in high contact stresses concentration on the tibial insert [DePuy, 2010]. Reducing such high concentrations is important to minimize polyethylene wear, ultimately reducing the incidence of total knee replacement (TKR) failure [DePuy, 2012]. Another feature of the femoral component aiding the reduction of polyethylene wear, are the extended posterior condyles, which allow 150° of flexion while maintaining contact with reduced contact stresses [DePuy, 2010]. Remarkably, the femoral component is made of a Cobalt-Chromium (Co-Cr) alloy, as this material

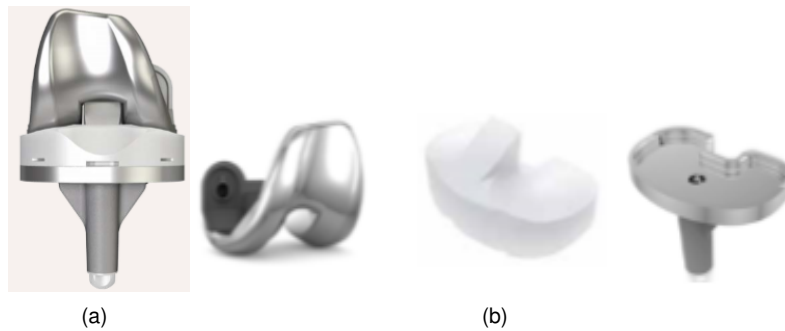


Figure 2.16: SIGMA<sup>®</sup> Posterior Stabilized Fixed Bearing Knee Prosthetic [DePuy, 2012] (a) and respective components used in primary surgery: Femoral Component, Tibial Polyethylene Insert and Tibial Tray, from left to right [DePuy, 2010] (b).

presents great resistance to wear.

Tibial trays can be made of either Co-Cr alloys or Titanium (Ti), with the latter being more prone to particle release. As this component is not as subjected to friction forces and wear as the femoral component, it is not as likely that such particles are released. As for the SIGMA<sup>®</sup> Fixed Bearing Tibial Tray, it is made of highly polished Co-Cr, as this material has been proven to show lower surface roughness and wear rates than its titanium counterparts [DePuy, 2012]. It is also polyethylene friendly, without compromising strength or fixation [DePuy, 2010], [DePuy, 2012].

The SIGMA<sup>®</sup> PS Tibial Insert, is designed out of XLK polyethylene, a moderately cross-linked and remelted polyethylene. Cross-linking by gamma irradiation improves the material's wear properties, particularly its resistance to multidirectional wear created by fixed bearing designs. Remelting above its melting point eliminates free radicals and makes the polyethylene oxidatively stable, which is important for avoiding mechanical failure and reducing wear rates [DePuy, 2010]. Shape wise, the PS Tibial Insert has a central elevated post, which articulates with the femoral component to substitute the PCL, by allowing femoral rollback. As a fixed bearing knee system, the tibial insert locks with the tibial tray. Micromotion between these two components is a concern, as it may have a negative effect on polyethylene wear rates. As a result, SIGMA<sup>®</sup> Fixed Bearing Knee Systems are designed with a locking mechanism with two prominent features. Firstly, the tibial insert is slightly larger (by 150 microns) than the tibial tray pocket, so that it must 'squeeze' inside the tray, thus avoiding rotational micromotion. Secondly, an anterior bumper is located between the two locking tabs, reducing the risk of breakage. It also absorbs anteriorly directed forces and reduces anterior/posterior micromotion, as a result [DePuy, 2010].

As for component fixation in TKA, the golden standard is cemented fixation, although uncemented fixation can also be performed, where bone ingrowth around the implant is encouraged. For cemented fixation, polymethylmethacrylate (PMMA) bone cement is used to form an interface between the bone and the prosthesis, by acting as a space-filler and creating a tight space, holding the implant against the bone [Vaishya et al., 2013]. An acrylic polymer, PMMA is the mixture of two sterile components, a liquid methylmethacrylate (MMA) monomer and a powdered MMA-styrene co-polymer. The two are mixed, resulting in an exothermic reaction and therefore, generating heat. Straight after mixing, PMMA is sticky, and its setting time is influenced by several factors, such as temperature, humidity and handling

method used. Lower temperatures increase the setting time, as do higher humidity levels. In terms of handling the cement, the mixing can either be performed manually or in vacuum, with the latter being recommended, as it reduces bone cement porosity and monomer evaporation [Vaishya et al., 2013].

#### **2.4.2.2 Revision TKA**

For revision surgeries, stems are added as a way of enhancing the stability of the knee joint, by improving the fixation of the prosthetic components to the respective bones. Moreover, these provide additional resistance to bending and torsion movements, reducing the load at the interface between the prosthetic components and the bones [Completo, 2006]. The SIGMA® PS Femoral Component can allow for the attachment of a stem collar through its intercondylar box. This collar, made of Co-Cr alloy, attaches to the femoral stem and can be adjusted so as to achieve the correct angle for the placement of the stem inside the intramedullary canal, with valgus options of 5° or 7° [DePuy, 2017]. The femoral stem considered in this study is the SIGMA® Universal Press-Fit Stem, with 125mm length and 14mm diameter, at 7° valgus.

The tibial stem used is the SIGMA® Universal Press-Fit Stem, compatible with the SIGMA® P.F.C. Modular Tibial Tray. Press-fit stems with different diameters and lengths are available. The tibial stem considered in this study is 14mm in diameter and 75mm in length. Both stems are made from Ti-6Al-4V titanium alloy and do not require the use of bone cement for fixation [DePuy, 2017].

### **2.4.3 Epidemiology**

Knee osteoarthritis (OA) is, currently, the leading cause of joint disability affecting the elderly throughout the world [Kim et al., 2008], with higher prevalence amongst females. Over the years, total knee arthroplasty has established itself as the most common management solution for late-stage knee osteoarthritis, in cases where OA causes permanent disability and symptoms cannot be controlled with other treatments [Jämsen et al., 2012]. Likewise, knee OA is the main indication for TKA, accounting for, in countries like Sweden, over 90% of total TKAs performed. [Jämsen et al., 2012, Robertson et al., 2010].

Ever since the initial development of the total knee arthroplasty in the early 1970s [Song et al., 2013], the number of TKAs performed each year has greatly increased. Notably, in the United States, TKA utilization has more than doubled between 1999 and 2008, with over 600000 TKAs performed in 2008 [Losina et al., 2012]. Similarly, in South Korea, the incidence of TKA doubled between 2002 and 2005 [Kim et al., 2008], while in Germany, an increase of 33% occurred between 2004 and 2008. Undeniably, population ageing leads to an increased number of patients suffering from knee OA, which contributes to an increase in the total number of TKAs. In fact, patients over the age of 65 constitute the great majority of TKAs performed. Interestingly enough, data shows that the greatest increase of TKAs performed, by age group, occurs in patients below 65 [Kim et al., 2012]. Similarly, in Norway and Sweden, between 1997 and 2007, the proportion of patients between 55 and 64 years old increased the most out of all age groups. This could result of an increased prevalence of obesity, which increases the need for arthroplasty in younger patients. Moreover, increased confidence in the longevity and results

of TKA may have convinced surgeons that it is a safe procedure for younger patients [Robertson et al., 2010].

Additionally, primary TKA incidence is higher for female patients, for all age groups. In nordic countries, for example, female patients account for over 60% of primary TKAs performed. In South Korea, however, the discrepancy is even higher, with TKA being 40% more likely to be performed on women [Kim et al., 2008]. The reasoning for consistently higher female incidence rates is still unknown. As for South Korea, women tend to resort to squatting positions for house chores, more often than men, which could result in higher risks of developing knee OA [Kim et al., 2008].

Overall, primary TKAs can be considered successful, as data shows that success rates exceed 90% at 10 years post-op [Robertson et al., 2010]. Undeniably, TKAs performed on younger adults are more likely to fail. In addition, younger adults are more likely to outlive the lifespan of their artificial joints. Until more robust components are developed, failure rates are likely to increase. As a result, revision rates are also likely to increase [Kim et al., 2012].

#### **2.4.4 Primary Total Knee Arthroplasty Surgical Technique**

Contemporary total knee arthroplasty demands high performance instrumentation to provide enhanced efficiency, precision and flexibility, with minimal invasion to the knee joint [DePuy, 2014]. The surgical technique for the implantation of SIGMA<sup>®</sup> Family of Fixed Bearing and Rotating Platform Knees is described below, in accordance with the information published by DePuy Shyntes Joint Reconstruction, a division of DePuy Orthopaedics, Inc. [DePuy, 2014].

Firstly, the skin is incised longitudinally, starting 2 to 4 cm above the patella, passing over it and ending at the tibial tuberosity (Figure 2.17(a)) [DePuy, 2014]. In order to expose the knee joint, the surgeon must choose how to perform the incision, from three possible approaches: the medial parapatellar; the mini-midvastus; or the mini-subvastus approach. The most commonly used approach is the medial parapatellar, in which an incision is performed through the retinaculum, the capsule and the synovium. The incision starts about 4 cm proximal to the patella, incising through the rectus femoris tendon longitudinally, continuing distally around the medial side of the patella, and stopping just above the tibial tuberosity, shown in Figure 2.17(b) [DePuy, 2014]. After the incision is performed, the patella is everted laterally, leaving the tibio-femoral joint exposed. As for the other two approaches, the process simply differs on the starting point of the incision.

After this, the surgeon performs the excision of hypertrophic synovium, if present, as well as a portion of the infrapatellar fat pad, in order to access the condyles and intercondylar space. This is followed by the removal of all osteophytes, which are bony projections that form along joint margins, so as to maintain soft tissue balance (Figure 2.17(c)). Particularly, removal of the posterior osteophytes should be thorough, as they may affect flexion and rotation of the femur [DePuy, 2014]. PCL resection is also performed at this stage.

The tibia is placed in flexion and anteriorly stabilized, in order to be resected, as shown in Figure 2.18(a). A cutting block is used, which must be aligned with the medial one third of the tibial tuberosity, so that varus or valgus misaligned cuts are avoided [DePuy, 2014]. The posterior slope at which the

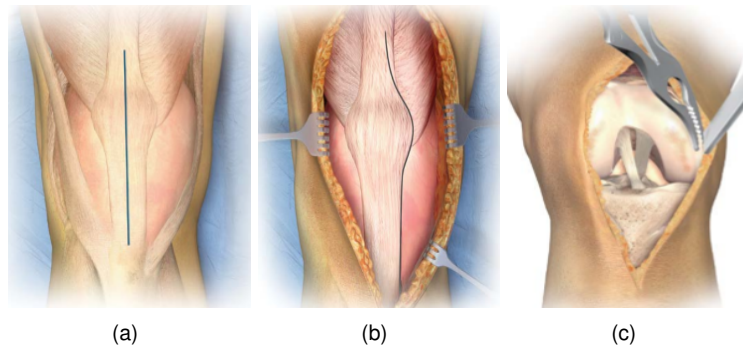


Figure 2.17: Midline skin incision (a), medial parapatellar incision (b) and osteophyte removal (c). [DePuy, 2014]

resection is performed is also important, and varies depending on the patient, ranging from 0 to 3 degrees in the sagittal plane. Tibial resection must be performed 8 to 10 mm below the more damaged side of the tibial plateau [DePuy, 2014]. As for the femoral alignment and distal resection, the medullary canal is made at the midline of the trochlea, 7 to 10 mm anterior to the PCL [DePuy, 2014]. As previously mentioned, while the tibial anatomical and mechanical axes are coincident, the femur's axes are not. Thus, the angle, which can range from 0 to 9 degrees, between the two must be defined pre-operatively, and set before the resection is done. Firstly, an intramedullary (IM) rod is inserted, after drilling at the midline of the trochlea, to a depth of approximately 5 to 7 cm. The rod is slowly introduced, to the isthmus level. The surgeon must be careful and avoid using excessive force to drive rod into the intramedullary canal. If resistance is encountered, the surgeon can decide to use a shorter rod. A femoral alignment guide is attached to the IM rod and the angle decide pre-operatively is set. The cutting blocks are then placed, and the medial/lateral placement is adjusted. Afterwards, the femoral alignment guide and IM rod are removed, and a resection of at least 9 mm of distal femoral bone from the most prominent condyle is performed (Figure 2.18(b)) [DePuy, 2014].

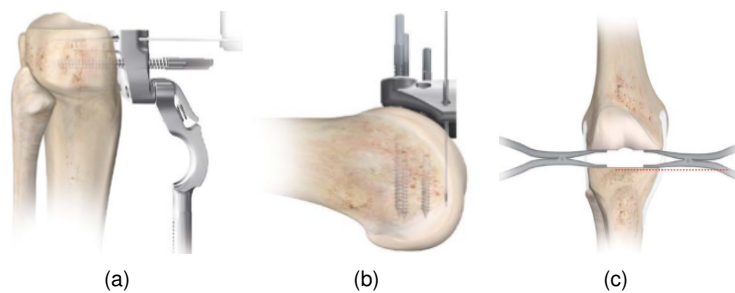


Figure 2.18: Proximal tibial resection (a), distal femoral resection (b) and extension gap assessment (c). [DePuy, 2014]

Following the distal resection, the extension gap must be measured (Figure 2.18(c)). In order to do so, spacer blocks are used. The extension gap must be rectangular. If not, soft tissue must be balanced in order to achieve the desired shape. At this point, femoral anterior and posterior resection is performed (Figure 2.19(a)), followed by notch and chamfer cuts (Figure 2.19(b) and (c)). Following that, the flexion gap is measured, to ensure it matches the extension gap.

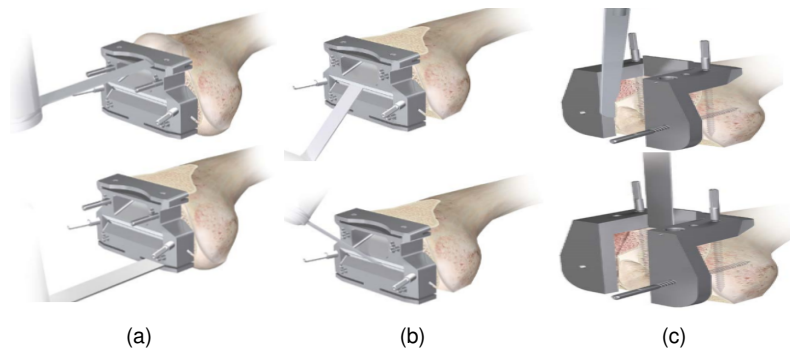


Figure 2.19: Anterior and posterior (a), chamfer (b) and notch (c) femoral cuts. [DePuy, 2014]

After all the preparation is done, the surgeon can test the prosthetic components, before inserting the final ones. Firstly, the femoral trial is performed, in order to find the right size component. Then, for the tibial trial, the tibial tray is chosen so that it matches, in size, the femoral component. Additionally, it must be positioned so that maximum tibial coverage is achieved, which usually occurs when the tibial tray is centered on the junction between the medial and central one-third of the tibial tuberosity. After the trial tray is inserted, the knee must be extended to assess stability and alignment in the anterior/posterior and medial/lateral planes. If instability occurs, the tibial tray must be replaced with the next greater thickness and the trial process repeated [DePuy, 2014].

Once the trials are completed, the components are removed, and a thick layer of bone cement is placed, either on the bone or the implants [DePuy, 2014]. The final components can be inserted, firstly the tibial tray, followed by the polyethylene component and finally, the femoral component. Any extruded cement must be removed. The subcutaneous tissue is then reapproximated and the knee is rotated from full flexion to full extension for the final time, in order to assess patellar tracking and the integrity of the capsular closing. Finally, the knee is ready to be closed [DePuy, 2014].

## 2.4.5 Complications

As previously mentioned, TKA is an overall successful intervention, with reports of clinical and radiographic success rates of greater than 90%, at 10 to 15 years follow-up [Tigani et al., 2015]. Nevertheless, although rare, complications may occur. Infection is the most feared complication, despite only occurring in a small percentage of cases. Rarely present in first time intervened knees, the incidence varies between 1 to 2% at 2 years post op, becoming higher in longer follow-ups, reaching 7% after revision surgery [Malizos and Varitimidis, 2017].

Overall, the prosthesis longevity is influenced by three main factors. The surgeon's technical expertise is the first and most determining factor. Secondly, the patient's activity levels influence the intensity of the loads the prosthesis will be subjected to. Finally, the bone's condition is also important. Naturally, an osteoarthritic or deformed bone is less likely to offer a good fixation to the prosthesis [Completo, 2006]. Any prosthesis is also vulnerable to experience wear, which inevitably aggravates with time. It is also influenced by the three main factors addressed previously. In extreme cases, fracture can also occur, as a result of the material's fatigue [Completo, 2006].

In the long-term, loosening is the most common complication that can occur. It consists of the relative movement between the prosthesis and the bone, which results in pain for the patient. It can occur in both cemented and non cemented prostheses. Additionally, incorrectly positioned components can also expedite loosening [Completo, 2006]. Loosening can also be caused by mechanical factors. If the bone tissue is damaged, it is unable to properly create an interface with the cement or the prosthesis. The bone's mechanical resistance is, therefore, compromised and the bone cannot withstand the stresses transmitted by the implant. It is unable to regenerate, which results in progressively larger implant instability. Loosening can also result from changes in the stress loads the bone is subjected to after implantation, as a result of the stress shielding effect. According to Wolf's Law, a bone adapts its structure according to the mechanical loads that it is subjected to [Completo, 2006]. Decreased stress leads to decreased remodelling activity, which leads to decreased stiffness, which can compromise bone stability.

Furthermore, loosening can also occur as a result of biological factors. If the components experience wear, particles can be released, triggering a response from the soft tissues surrounding the joint. This response will degrade the bone tissue, which is substituted by fibrous tissue, and cause loosening [Completo, 2006].

## **2.4.6 Revision Total Knee Arthroplasty**

As a result of the possible complications mentioned, revision surgery is a necessity for some patients. Furthermore, the increasing number of patients subject to primary TKA, the expansion of the procedure to younger and more active patients, the implant's longevity and the modifications in surgical technique are all factors that contribute to the increased number of revision TKAs performed. [Tigani et al., 2015]. Most commonly, revision surgery is indicated when component loosening, wear, infection or instability occurs [Tigani et al., 2015], [DePuy, 2013].

Revision surgery is closely linked to bone loss, which is inevitable after a primary TKA, whether as a result of inflammatory processes, or due to the stress shielding effect caused by the implant. In some cases, bone loss can be so pronounced that bone grafts or metallic augmentation components must be used. To that end, when choosing the replacement components, one must bear in mind that stability is a focal point of the surgery. Therefore, the components must offer the best possible attachment to the areas where bone was replaced or resected once more. Oftentimes, the primary components alone are unable to offer the required stability, hence the use of stems, which help the fixation of the components. Furthermore, stems are also responsible for reducing the load on the bone/implant or bone/cement interface [Completo, 2006].

### **2.4.6.1 Revision Total Knee Arthroplasty Surgical Technique**

In pre-operative planning of a revision surgery, the main goals must be the restoration of the anatomical alignment and functional stability, the fixation of the revision implants and the accurate re-establishment of the joint line. Planning involves a physical examination of the soft tissues, and takes into account factors such as previous skin incisions, range of motion, motor strength, the condition of all

neurovascular structures, ligamentous stability and the integrity of the extensor mechanism. In addition, radiographic views, and sometimes MRI scans, are obtained for the assessment of alignment and bone stock, documentation of the joint line and evaluation of the present implant fixation [DePuy, 2013]. The surgery involves, if necessary, the removal and replacement of damaged prosthetic components or the entire prosthesis. Considered a more complex surgery when compared to primary TKA, revision surgery presents higher risks of infection. The surgical technique for the implantation of the SIGMA<sup>®</sup> Knee Revision System is described below, in accordance with the information published by DePuy Shyntes Joint Reconstruction, a division of DePuy Orthopaedics, Inc. [DePuy, 2013].

The initial skin incision must follow, as much as possible, the incision from the primary procedure. The same occurs for the capsular incision and eversion of the patella, in order to expose the extensor mechanism (Figure 2.20(a)). Ensuing, the primary components are carefully removed, so as to maximize the amount of bone preserved. The bone/cement or bone/implant interface must be disrupted prior to attempting extraction, so that fracture or bone stock loss is avoided. Notably, when removing the entire prosthesis, the femoral component is removed first, granting better access to the tibial component. At this stage, residual cement must be removed, as shown in Figure 2.20(b).

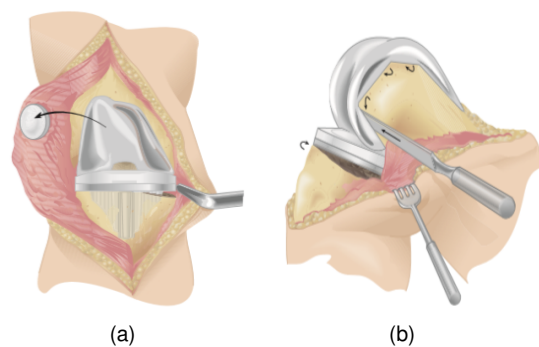


Figure 2.20: Exposure of the extensor mechanism (a) following the medial patellar incision and patellar eversion, Disruption of the bone/cement or bone/prosthesis interface (b) before attempted extraction [DePuy, 2013].

Subsequently, the surgeon should assess the level of the joint line. Ideally, this should be one finger's width below the inferior pole of the patella [Tigani et al., 2015]. The flexion/extension gap relationship is also assessed, as well as its symmetry, as extension (2.21(a)) and flexion (2.21(b)) gaps must be, at all times, equal. This is done with resource to spacer blocks, similarly to the primary surgery, and is an essential step to determine whether the prosthetic components' size must be altered, in case of gap size discrepancy [DePuy, 2013]. If the knee is loose in flexion, the femoral component must be upsized with posterior augmentation [Tigani et al., 2015]. If loose in extension, the distal femur must be augmented with bone graft or prosthetic augmentation [DePuy, 2013].

When a stem extension is required to increase fixation, it is recommended that the proximal tibia be prepared with reference to the position of the IM rod. The knee is placed in maximal flexion and the intermedullary canal is made with the use of a drill, to a depth of 2 to 4 cm, avoiding cortical contact. Reaming depth is determined by the length of the fluted stem, and the canal is progressively reamed until firm endosteal engagement is established, with the final reamer indicating the diameter of the

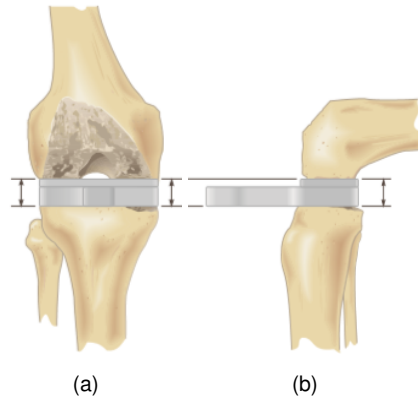


Figure 2.21: Extension gap (a) and Flexion gap (b) of the Revision TKA [DePuy, 2013].

implanted fluted stem [DePuy, 2013]. Proximal tibial resection is performed as minimally as possible, in order to avoid losing bone stock, as this has already been sacrificed in the primary surgery. The femoral preparation begins by drilling the intermedullary canal, with a 9mm drill, to a depth of 3 to 5 mm, followed by reaming, similarly to the tibia. This is followed by distal resection, if necessary to establish a viable surface, as well as anterior and posterior, and notch and chamfer resection. Finally, the knee is placed in full extension to determine the appropriate rotation of the tibial tray. The tibial trial is performed with the tibial tray and tibial stem assembled, after which rotation and proximal tibial coverage are assessed [DePuy, 2013]. Afterwards, the final tibial tray and tibial stem can be assembled. Next, the femoral component and femoral stem assembled together with the help of an stem bolt. The stem bolt can be adjusted according to the desired inclination of the stem. The femoral trial is performed to assess the femoral component is placed with the correct rotation.

With this confirmation, the trial components are removed in reverse order and the site is thoroughly cleansed. When using fluted stems, one must ensure there is no cement present in the intermedullary canals. Implantation begins with the tibial tray and stem, followed by the femoral component and respective stem, finishing with the tibial insert. Finally, the knee is closed, similarly to the primary surgery [DePuy, 2013].



## Chapter 3

# Implementation

The success of knee replacement surgeries is deeply correlated with the understanding of the knee's biomechanical behaviour, as previously mentioned in Section 2.3. Computational models of these prosthetic replacements, where the anatomical structures and prosthetic components are included, have become essential to analyze the movements, forces and stresses that affect the knee in a variety of different activities [Completo, 2006]. As such, not only do these models provide great help during the design phase, but they can also provide an indication of expected clinical performance [Halloran et al., 2005], allowing a more personalized and effective treatment plan for the patient.

The complexity of the anatomical structures involved is one of the major difficulties encountered when developing 3D anatomical models. Thus, the field of medical imaging has played a major role in the development of such numerical models. Medical imaging techniques such as Magnetic Resonance Imaging (MRI) and Computed Tomography (CT) Scans, are essential to obtain simulations with great anatomical and physiological accuracy [Completo, 2006, Ribeiro et al., 2009]. An exciting application for 3D anatomical models is, in particular, finite element analysis (FEA), as it can be applied to the study of bioengineering problems. In particular, it can provide relevant data for increasing the probability of successful therapeutic treatments, as well as improving surgical planning and injury prevention [Ribeiro et al., 2009].

In this chapter, the implementation process used for the 3D models design is thoroughly described, starting with the acquisition of the CT knee images. Following that, the segmentation and smoothing process and the 3D CAD modelling and assembly processes are also described in detail. Finally, the methodology for the creation of the numerical models, with resource to a finite element analysis software, is described, including the definition of the mechanical properties, the contact and boundary conditions and the loading conditions applied, as well as the finite element mesh generation.

### 3.1 Bone Images Acquisition

It is known that different medical imaging techniques are based on different physical principles, which provide characteristic *in vivo* image data for different tissue types within a body section [Ribeiro

et al., 2009]. In other words, one can choose a certain imaging modality by knowing which types of tissues one wants to analyze. In this case, in order to visualize bone, a hard tissue, Computed Tomography is the most appropriate technique. CT is an imaging technique based on X-ray radiation, which is absorbed differently by various tissues, based on tissue density. These density variations can be quantified by the attenuation coefficient or Hounsfield unit (HU). As hard tissues greatly attenuate high energy radiation, these appear in the image with a high signal [Ribeiro et al., 2009]. This equates to a high contrast between bone and soft tissues, such as fat, muscle and cartilage. Soft tissues all show low signal intensity, and because of small differences in attenuation, also show low contrast, making it difficult to distinguish between each of them in a CT image. Therefore, when one wants to study soft tissues, MRI images are more appropriate, as these present a high soft tissue contrast [Ribeiro et al., 2009].

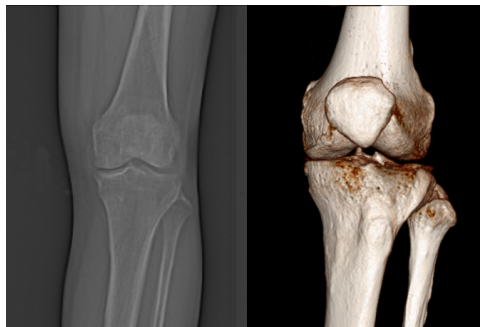


Figure 3.1: Topogram and VRT (Volume Rendering Technique) CT image of the female left knee joint CT images.

The CT images used, kindly provided by Dr. Gamelas, show a female left knee, as shown in Figure 3.1. These 253 images were saved in Digital Imaging in Medicine and Communications (DICOM) format and used for the bone segmentation process, performed through ITK-SNAP.

## 3.2 Bone Segmentation Process

The bone segmentation was performed on the free, open-source and multi-platform software ITK-SNAP (version 3.8.0, 2019) [Yushkevich et al., 2006]. Image segmentation can be defined as a partition of an image into non-overlapping regions, in which each region is the locus of an object [Ribeiro et al., 2009]. As a result, this technique allows to delimit, from medical images, the desired anatomical structure one wishes to study.

In order to segment the bones that constitute the knee joint, three techniques are used in conjunction: global thresholding, active contour method and manual segmentation [Ribeiro et al., 2009]. Firstly, one must start by defining a region of interest on the three anatomical planes for the segmentation, as exemplified in Figure 3.2. Global thresholding can then be performed, where the intensities of the tissues are defined, creating boundaries between the desired tissue (image foreground) and the rest (image background). The values represent the Hounsfield values of each voxel. Therefore, by partitioning an image into regions according to the voxel intensity value, usually, a segmented object will appear.

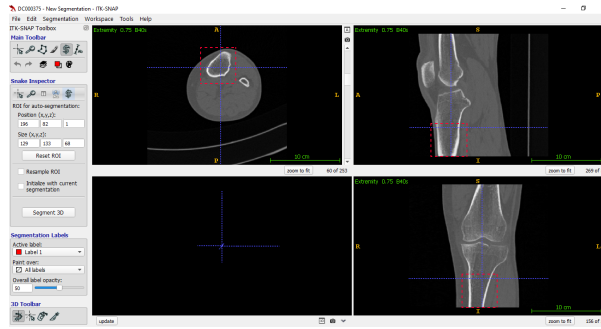


Figure 3.2: Definition of the 3D region of interest for segmentation on ITK-SNAP.

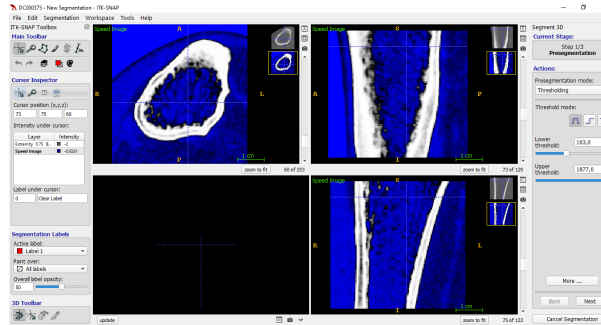


Figure 3.3: ITK-SNAP Active contour segmentation mode definition of threshold values.

In this case, bone must appear in the foreground. As it has a high intensity value, the upper limit of thresholding should be set to the maximum value and the lower limit should be set so that a clear outline of the bone is obtained, as shown in Figure 3.3. However, due to partial volume effect, the established intensity interval encloses not only bone tissue but also muscle, fascia and bone marrow [Ribeiro et al., 2009].

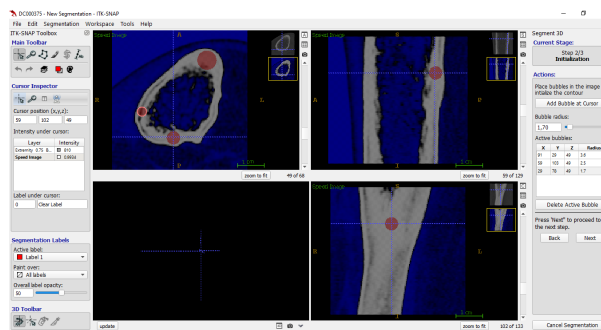


Figure 3.4: ITK-SNAP Active contour segmentation mode placement of the spherical surfaces.

After thresholding, active contour can be applied. This semi-automatic method is based on deformable models, called snakes. A tissue can be outlined by placing an initial set of closed spherical surfaces, in the proximity of the region of interest, shown in Figure 3.4 [Ribeiro et al., 2009]. Through an iterative process, these surfaces deform in a way that fills up the foreground, that is, delimits the desired anatomical structure, as shown in Figure 3.5. The results obtained might show segmentation errors, which must then be corrected by manual segmentation. In this mode, the user can manually correct the regions that are to be segmented, closing holes and improving outlines, for example. Such a process

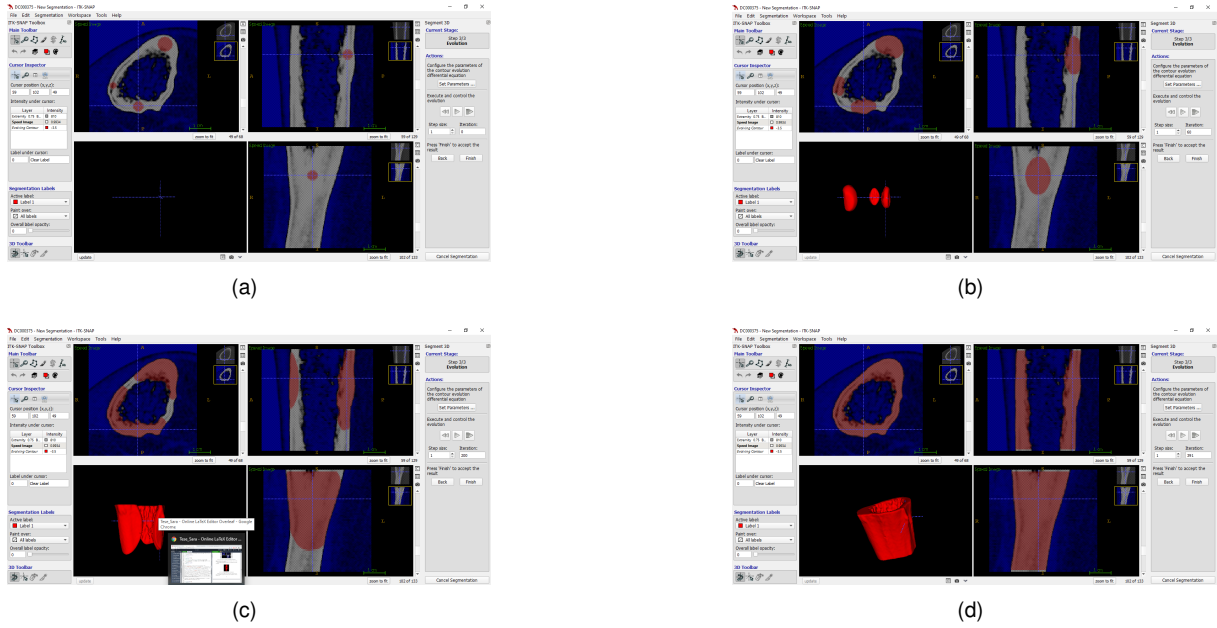


Figure 3.5: ITK-SNAP Iterations of contour evolution of the semi automatic segmentation mode, (a) before initiation, (b) after 60 iterations, (c) after 200 iterations and (d) after contour is complete.

requires, of course, a thorough knowledge of the anatomical characteristics of the desired structure. In the end, ITK-SNAP exports the anatomical model as a 3-D surface mesh using the marching cubes algorithm. In Figure 3.6(a), the tibia is not aligned with the femur in an anatomically correct manner. This does not pose a problem, as it can be corrected later on, by being internally rotated. The segmentation process was also performed to obtain a model for the fibula (Figure 3.6(b)), which is assembled with the remaining bones in a posterior phase.

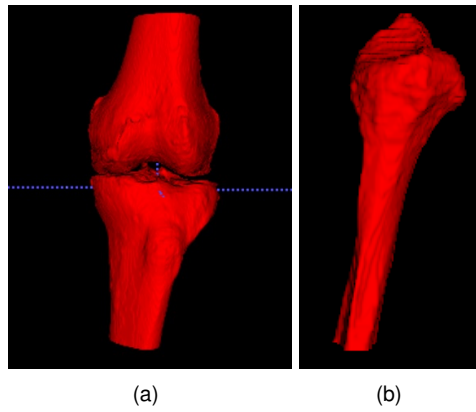


Figure 3.6: Final ITK-SNAP segmentation model of (a) the left tibia and femur and (b) left fibula.

### 3.3 Smoothing Process of the Segmentation Results

The output of the segmentation process is a binary volume, with the anatomical structure of interest in voxel format [Ribeiro et al., 2009]. ITK-SNAP then generates a triangular 3D surface mesh, with the use of the marching cubes algorithm. After the segmentation process is completed, the surface

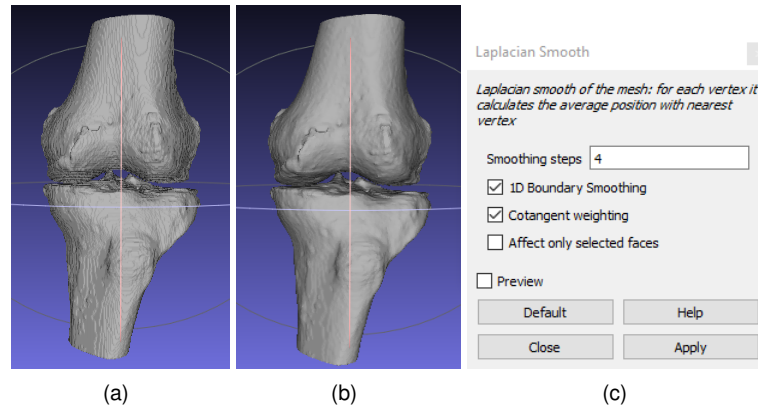


Figure 3.7: 3D knee joint model before and after applying Laplacian Smooth Filter, with 4 smoothing steps.

model is exported as an STL file to a smoothing software. The chosen software for this step was Mesh-Lab (version 1.3.4BETA). In this software, processing occurs by applying a low pass filter to the surface mesh, improving it by smoothing the stair-step shape curvature and removing irrelevant and excessive nodes and facets, both characteristic limitations of the marching cubes algorithm [Ribeiro et al., 2009]. A Laplacian smooth filter is applied, as shown in Figure 3.7(c) and the model is exported as a point cloud (.xyz) file. This file is then imported into Computer-aided design (CAD) software SolidWorks® (version SP02, 2019), in which the 3D bone solid models are created, with resource to its ScanTo3D® toolbox.

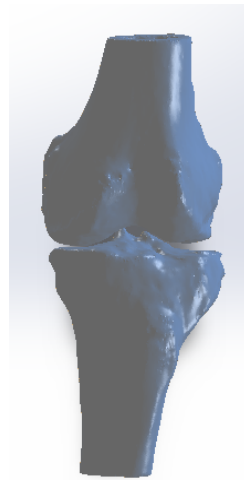


Figure 3.8: Original Mesh obtained with the ScanTo3D toolbox in SolidWorks®.

### 3.4 Geometric Modelling and Assembly Process

The Point Cloud file was uploaded to SolidWorks®, where the ScanTo3D® toolbox was used to form two surface bodies, as shown in figure 3.8. When working with Point Cloud files, it is common to find plenty of flaws in the created surfaces. As these pose problems when creating meshes for the FE numerical models, two solid bone models were created, with the use of the Loft surface tool. From the original mesh, various intersection curves were created, parallel to the frontal plane. Perpendicular

guide curves were created as well, so that the loft would follow, as much as possible, the original shape of the bones. Furthermore, the CT images did not include much of the bones' diaphyses. Hence, when creating the lofts, instead of stopping at the same location as the segmentation, extensions along the length of the diaphyses were added. These extensions were based on the SolidWorks® files from a previous work, which followed the same methodology for creating solid bodies from CT images of a female left knee [Moreira, 2018]. From these, the ratios of the external diaphysis diameter along the length of both bones' diaphyses were considered, in order to avoid mistakes resulting from differences in bone size.



Figure 3.9: Computational 3D Solid Model of the knee joint using the SolidWorks® Loft Surface Tool, based on the original mesh obtained with the ScanTo 3D® toolbox.

The tibial resection was also performed at this stage, 10mm distal to the tibial plateau and parallel to the mechanical axis of the tibia [DePuy, 2014]. This distance was measured from the tibial plateau of the original surface mesh, as the approximate lofted bone did not include the entire tibial condyles. These were not fully included as, firstly, that would difficult the loft design. Secondly, as the theoretical information on the surgical technique shows in Subsection 2.4.4, it was already known that the tibial condyles would be resected, prior to the creation of the lofted tibia. Therefore, as the tibial surface mesh and lofted tibia are coincident, the 10mm were measured vertically from the theoretical tibial plateau, and resected accordingly from the solid bone model. The anterior slope of the knee was also considered, thus the cut was performed with a 3° slope on the anterior-posterior plane. Since, in theory, the CT images used show a knee with the proper size to fit the prosthetic components used in this

study, no scaling of the bones was necessary. The 3D bone models obtained are shown in Figure 3.9. Separately, the fibula model was imported into SolidWorks®, where it was also converted to a surface body through the ScanTo3D® toolbox. Similarly to the tibia and femur, the fibula was also transformed into a solid body through the Loft surface tool. In order to be compatible with the other bones, the fibula was extended to about the same length as the tibia, as shown in Figure 3.10.



Figure 3.10: Frontal view of the Computational 3D Solid Model of the fibula using the SolidWorks® Loft Surface Tool, based on the original mesh obtained with the ScanTo3D® toolbox.

As for the geometric modelling of the prosthesis, it is important to note that the computational 3D models of the components used had already been obtained in a previous work [Moreira, 2018]. These SolidWorks® Part files were reused, as they were considered relevant to this study. Nevertheless, it is worth mentioning how these files were created. As the prosthetic components display complex surface geometries, a 3D scanner was required to create the initial digital models of both the femoral and polyethylene components. The defects and artifacts present in these models' surfaces were corrected on SolidWorks®, using again its ScanTo3D® toolbox [Moreira, 2018]. As for the tibial component, the 3D model building was divided into two steps. Firstly, to build its overall shape (including the keel design and tray thickness), the physical model was used as a basis. Then, for the design of the tibial tray outline, the polyethylene 3D model was used as a basis, to ensure both had the same shape and size, enabling them to be assembled [Moreira, 2018]. The resulting 3D models of the knee prosthesis are shown in Figure 3.11.

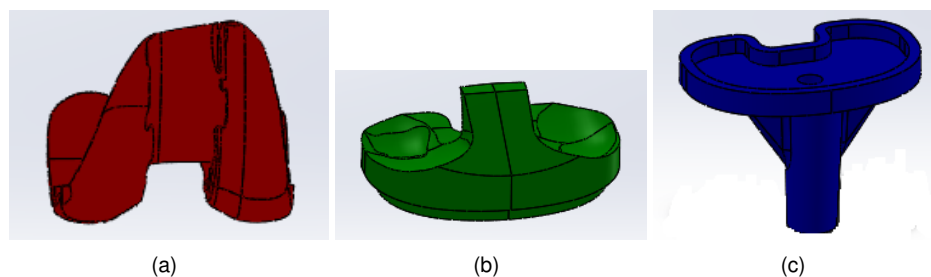


Figure 3.11: Computational 3D models of the (a) Femoral Component, (b) Tibial Insert and (c) Tibial Tray of the SIGMA® PS Fixed Bearing knee prosthesis [Moreira, 2018].

The fluted stems used in revision surgeries were also subjected to 3D modelling on SolidWorks®, based on the physical models of the femoral and tibial stems, with a diameter of 14mm and a length of 175 and 75mm, respectively. For the femoral stem, in particular, small modifications had to be done on its original design, so that compatibility with the modelled femur was ensured, as it did not include the entire diaphyseal length. Specifically, the stem was shortened to accommodate this limitation. Furthermore, the configuration of the distal end of the stem and bolt designs was altered [Moreira, 2018]. An additional set of stems were designed to create the intermedullary canals where the stems are placed, in the revision surgery models. These stems were slightly modified, in order to ensure that no bone was left in the canals after their creation. Both sets of stems are presented in Figure 3.12.

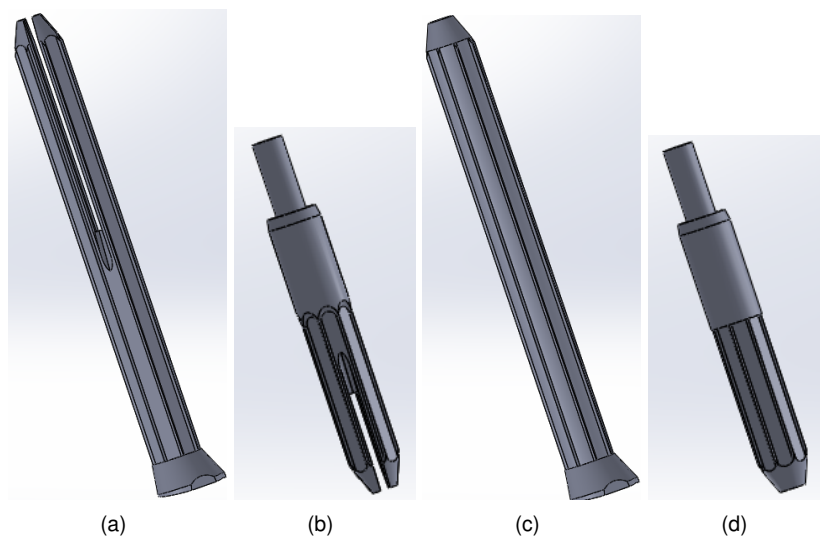


Figure 3.12: Computational 3D models of the (a) Femoral and (b) Tibial Stems and of the modified (c) Femoral and (d) Tibial stems, used for the creation of the intermedullary canals [Moreira, 2018].

Once all 3D components were obtained, the assembly process was initiated. At this stage, the tibia was internally rotated in order to achieve proper alignment, with the tibial tuberosity positioned more anteriorly. In order to study the primary surgery case, one of the 3D models was assembled without any stems. As for the revision surgery, all possibilities had to be studied. Thus, 3 models were created, one with a tibial stem only, one with a femoral stem only, and one with both. Firstly, in order to get the right positioning of the prosthesis, the assembly began by positioning the stems in the bone canals. This ensures proper alignment, as the stems should follow the direction of the intermedullary canal. Once the alignment is guaranteed, the tibial tray and polyethylene insert are assembled, as well as the femoral component. As for the femur, the femoral resection cuts were performed as a complement to the femoral component, using the Cavity feature in SolidWorks®, which keeps both bodies, subtracting the parts of the bone overlapping the prosthetic component.

In order to obtain distinct cortical and trabecular bone regions, trabecular bone portions of the femur and tibia were created as solid bodies, positioned inside the full solid bone models. As a guideline, Solidworks® files of scanned medical training bones were used, as a way of assessing the thickness of the cortical outer layer along the bone. These training bones are produced by SAWBONES® and are used for *in vitro* testing of load conditions for the development of medical devices. Knowing that, on an

epiphyseal level, the bones are mostly comprised of trabeculae and that along the diaphysis, the cortical part thickens, a new loft inside each bone was created, representing the trabecular bone. Furthermore, the design of the new loft also took into consideration the positioning of the stems. In *in vivo* surgical procedures, the stems are positioned so that they follow the intermedullary canal, and, in the case of press-fit stems, firm endosteal engagement is established [DePuy, 2013]. The cortical bone regions are created later on, in ABAQUS®. The solid bone models, including the trabecular solid bodies, are shown in Figure 3.13.

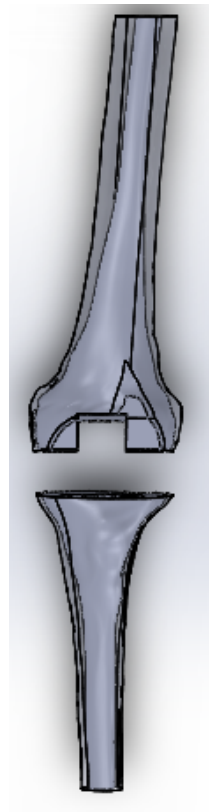


Figure 3.13: View of the fully filled bone models and the trabecular bone models displayed on SolidWorks®.

Since the fibula does not play an important role in the load distributions of the knee joint, an internal trabecular component was not considered. Instead, the fibula was considered as a single solid body, composed of cortical bone. In regards to the assembly, although it does not attach to any other bone, the fibula was properly positioned in the SolidWorks® assembly. The connections between the fibula and the femur and tibia, assured by the LCL and the Posterior Tibiofibular Ligament (PTL), respectively, are performed later on in the study. Once the final 3D computational models, shown in Figure 3.14, were obtained, they were exported as Parasolid format files to ABAQUS® (2020 version), a software suited for finite element analysis.

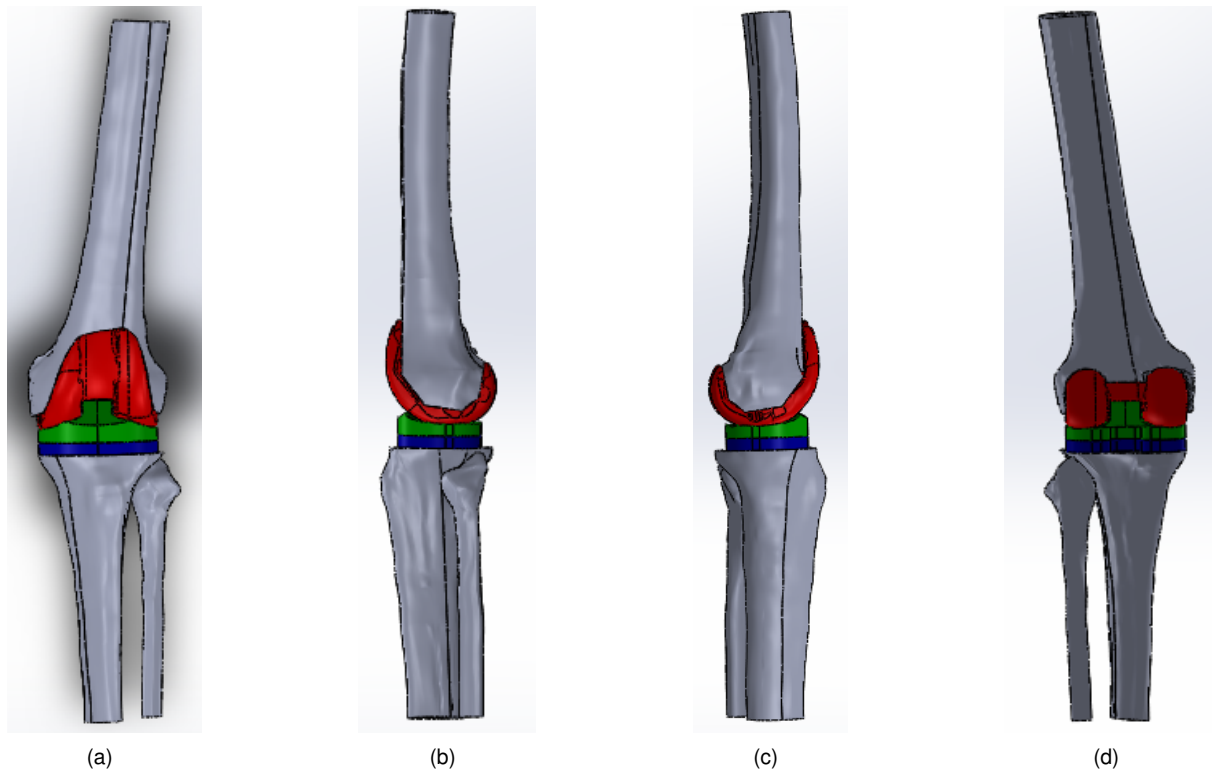


Figure 3.14: Anterior (a), Lateral (b), Medial (c) and Posterior views of the 3D computational model of the knee joint with insertion of the SIGMA<sup>®</sup> Fixed Bearing knee prosthesis, Cortical and trabecular bone displayed on SolidWorks<sup>®</sup>.

### 3.5 Numerical Modelling and Finite Element Analysis

The 3D computational models are used for the creation of numerical models, which are analyzed through the Finite Element Method (FEM). FEM is a computational numerical model, widely used in engineering for the solving of complex problems, as well as for the design and manufacturing of high-technology products, such as medical prostheses [Reddy, 2005]. In the FEM, a complex structure is divided into smaller, simpler structures, called the finite elements (FE). The elements are created by the generation of a mesh and are interconnected by nodes. As a result, an approximated solution for the complex problem can be found, as a combination of the solutions of simpler problems [Completo, 2006].

In the field of orthopaedic biomechanics, FEA has been widely used to analyze the mechanical behaviour of biological tissues, such as bones, muscles and cartilages. Particularly, FEA allows the study of stress-strain rates for these tissues, which is relevant for the study of biological processes, such as bone growth and remodelling processes, as well as fracture healing processes. Furthermore, and most importantly for this study, FEA can also be applied to the study and development of prostheses and orthopaedic devices, in order to achieve optimized performances and predict surgical outcomes [Completo, 2006].

### 3.5.1 Mechanical Properties of the Materials

Once the numerical models were imported into ABAQUS<sup>®</sup>, the cortical bone portions were created, resorting to the Cut tool, which was used to create a cavity in the full bone solid bodies, coincident with the trabecular bone. Ensuing, the cortical and trabecular bone models were merged, creating a single bone part with distinct cortical and trabecular portions. In addition, at this point, the intermedullary canals were created for the revision models, using the Cut tool once more. Afterwards, the mechanical properties of each component were defined.

It is well known that bone is not an homogeneous material and that the bone stress distributions are correlated with the bone density values. Thus, in computational studies of this nature, specific software is commonly used to extract information from CT images, in Hounsfield Units (HU), which are ultimately converted to bone density values. However, in order to get accurate nodal density values, the node coordinates of the CT images and the final bone models must match. In this particular case, the final 3D bone models are approximations of the bone models obtained from the CT images. Furthermore, rotations were applied and extensions were added, meaning that, if such software were to be used, not only would there be locations of the bone models with wrong densities associated to them, the extensions would have null bone density values.

Thus, for simplification purposes, the bone was defined as a linear elastic, isotropic and homogeneous material. In accordance with the previous decision to divide the bone into sections of cortical and trabecular bone, two materials with different Young's Modulus ( $E$ , in MPa) were defined. The Poisson's Ratio was considered the same for both materials. In order to define the values of material parameters for the trabecular and cortical bone, information on composite bones used for *in vitro* testing was considered. According to SAWBONES<sup>®</sup>, these composite bones are produced with an outer layer of short fiber filled epoxy resin (to simulate cortical bone), and are filled with a uniform structure of solid rigid polyurethane foam (to simulate trabecular bone). Defining bone material properties according to these composite bones has been previously done in studies of this nature, and the values of such parameters do not qualitatively affect the results of the analysis performed, due to the comparative nature of the study [Completo, 2006]. Notably, these different bone materials were considered for the femur and tibia. As for the fibula, only cortical bone was considered, as previously mentioned.

Finally, FE models of the LCL and MCL were created, in a similar fashion to the work of [Moreira, 2018], with a wire shape and tension-only truss sections. These were defined with the cross-sectional areas presented in Table 3.3 and assembled to the complete knee joint FE model. The ligaments were also modelled with a 2% prestretch [Liacouras and Wayne, 2007].

Notably, a simplified version of the combined anterior and posterior proximal tibiofibular ligament (PTL), responsible for connecting the tibia and fibula, was modelled. Three springs, with a stiffness of  $k=10^6\text{N/m}$  were created, in order to model the PTL. Each spring was modelled to prevent displacement in each of the three translational degrees of freedom. All ligaments were connected to the bone models by Coupling interactions, with attachment surfaces being defined for each ligament insertion point, shown in Figure 3.15. By using this type of interaction, and selecting a continuum distribution, the forces are

uniformly distributed onto the surface. The locations of each insertion point and the area of the respective attachment surface, were taken from literature, and are shown in Table 3.3.

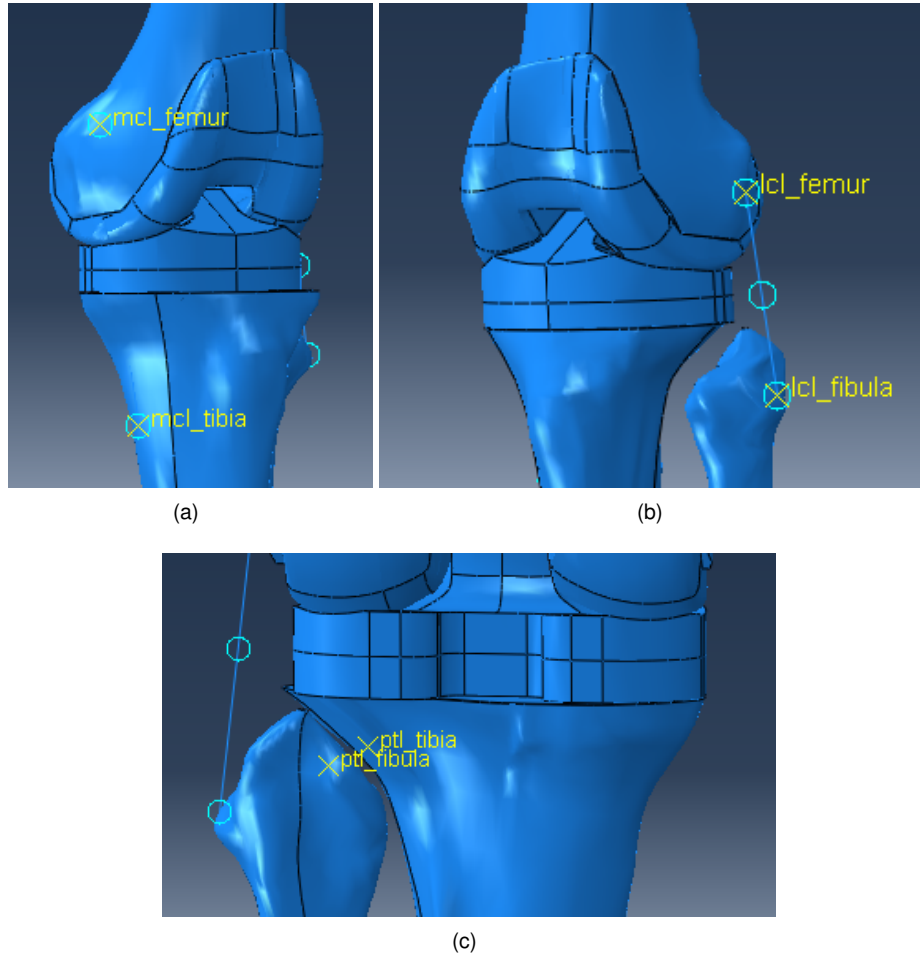


Figure 3.15: Insertion points of the (a) MCL, (b) LCL and (c) PTL ligaments, in the FE model.

Each prosthesis component was assigned its corresponding material, parameterized by the values of the Young's Modulus and Poisson's Ratio, obtained from literature. Each material was defined as linear, elastic and isotropic, as well. In summary, all the material properties and parameters assigned to each part of the model (including the femoral and tibial stems), are presented in Table 3.1.

### 3.5.2 Contact and Boundary Conditions

Ensuing, the interactions and constraints between the different elements of the assembly were defined. In particular, since cement was not modelled, bone and prosthetic components were bonded. For the tibial component, a Tie constraint was used, between the tibial tray inferior surface and the resected tibial surface. As for the femoral component, a surface-to-surface contact with cohesive behaviour properties was chosen. The stiffness coefficients used were uncoupled. Since bone cement has a Young's Modulus of approximately 3GPa [Vaishya et al., 2013], the values considered for the stiffness coefficients were  $K_{nn}=3000$ ,  $K_{ss}=1500$  and  $K_{tt}=1500$ .

A Tie constraint was also used to bond the tibial polyethylene insert and the tibial tray, as the two

Table 3.1: Material type and the corresponding properties and parameters (Young's Modulus and Poisson's Ratio, attributed to the final FE model of the knee joint, prosthetic components and stems).

	Model Part	Material Type	Material Property	Young's Modulus $E$ (MPa)	Poisson's Ratio $\nu$	References
Bones	Femur	Cortical Bone	Elastic, Isotropic and Homogeneous	17000	0.3	[Heiner, 2008]
		Trabecular Bone		1000		[Ryan and Williams, 1989]
	Tibia	Cortical Bone		17000		[Heiner, 2008]
		Trabecular Bone		1000		[Ryan and Williams, 1989]
	Fibula	Cortical Bone		17000		[Heiner, 2008]
Ligaments	LCL	Ligament	Elastic and Isotropic	493.86	0.4	[Cho and Kwak, 2020],
	MCL			326.75	0.4	[Orozco et al., 2018]
Prosthesis	Femoral Component	Co-Cr Alloy	Elastic and Isotropic	210000	0.36	[Eidel et al., 2020]
	Tibial Insert	XLK Polyethylene		900	0.46	[Kang et al., 2019]
	Tibial Tray	Co-Cr Alloy		210000	0.36	[Eidel et al., 2020]
	Femoral Stem	Titanium (Ti-6Al-4V Alloy)	Elastic and Isotropic	110000	0.33	[Eidel et al., 2020]
	Tibial Stem					

components are designed with a locking mechanism, as previously mentioned. For the bone-implant contacts where no cement is applied, such as the contact between the tibial keel and the tibia, as well as the contacts between the press-fit stems and the bone canals, a coefficient of friction of 0.3 was used [Viceconti et al., 2000, Robalo, 2011]. The types of interactions and constrains, and the friction coefficients chosen, when applicable, are described in Table 3.2. In addition, both the distal tibial and fibular ends were pinned with the boundary condition "Encastre".

Furthermore, since the femoral component and tibial insert were not connected, it was necessary to constrain the FE model so that the numerical model could converge. Thus, six springs with a stiffness of  $k=10^6\text{N/m}$ , were added to the model with the goal of constraining movement in all six degrees of motion (3 translational and 3 rotational). Each spring was connected to two overlapping reference points, one coupled with the femoral component surface and the other coupled with the tibial insert surface. Both Coupling interactions were modelled with continuum distribution and uniform weighting, represented in Figure 3.16.

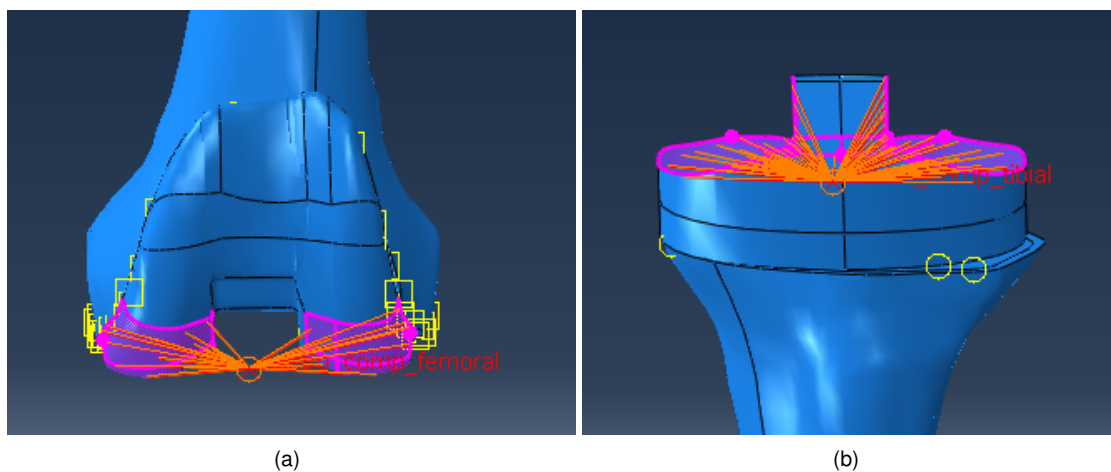


Figure 3.16: Coupling interactions between the prosthetic surfaces and the springs.

Table 3.2: Interactions and constrains applied to the FE models with insertion of the primary prosthesis components and, when applicable, of stems. Indication of the friction coefficient values when applicable.

Model Parts	Interaction/Constraint Type	Friction Coefficient	References
Tibia - Tibial Keel	Surface-to-Surface Contact	0.3	[Viceconti et al., 2000], [Robalo, 2011]
Tibia - Tibial Tray	Tie		
Tibia - Tibial Stem	Surface-to-Surface Contact	0.3	[Viceconti et al., 2000], [Robalo, 2011]
Femur - Femoral Stem	Surface-to-Surface Contact	0.3	[Viceconti et al., 2000], [Robalo, 2011]

Table 3.3: Description of the FE models of the knee joint ligaments, including their cross-section area, the interaction between their insertion points and the bones, and their influence radius.

Ligament	Bone	Ligament Cross-Section Area ( $mm^2$ )	Constraint Type between the Ligament and the Bone	Influence Radius of the Insertion Point ( $mm$ )	References
LCL	Femur Fibula	8.76	Coupling	7 6.5	[Cho and Kwak, 2020] [LaPrade et al., 2003]
MCL	Femur Tibia	24.54	Coupling	9 15	[Cho and Kwak, 2020], [Liu et al., 2010]
PTL	Tibia Fibula	N/A	Coupling	6.4 9.7	[Hermans et al., 2010]

### 3.5.3 Load Conditions

In order to recreate as closely as possible the loading that a real knee is subjected to, two groups of forces were applied to the FE model, the joint reaction forces and the muscle tendon forces.

Firstly, the joint reaction forces were obtained from the free public data base, OrthoLoad. These forces are measured through the use of instrumented implants and are based on the study by [Kutzner et al., 2010], where forces and moments acting on the tibial component during daily living activities are measured *in vivo*. For this study, six loading cases corresponding to six instances of the walking gait cycle were considered. Since the forces were measured on a 100kg male's right knee, conversions were made to fit a 70kg female's left knee. Furthermore, since the model in this study contains not only a tibia, but also a femur, the application point for these reaction forces and moments was altered, to a reference point coupled to the uppermost surface of the femur. Both the original and the femoral surface application point are shown in Figure 3.18. Considering the model to be at static equilibrium, the forces applied at the center of the tibial component remain the same at the femur surface. However, the new moment values must account for the distance to the center of the tibial component. Thus, a vectorial

product was used to determine the new moment values, resulting in the following equation system 3.1.

$$\begin{cases} M'_x = M_x + F_z d_y - F_y d_z \\ M'_y = M_y + F_x d_z - F_z d_x \\ M'_z = M_z - F_x d_y + F_y d_x \end{cases} \quad (3.1)$$

As for the muscle forces, four muscles were considered: the bicep femoris (BF), the semimembranosus (SM), the TRIPOD (a combination of the sartorius, gracilis and semitendinosus muscles), as well as the distal portion of the quadriceps femoris tendon, known as the patellar tendon (PT). Insertion sites were modelled as reference points (Figure 3.17), coupled to the tibial anterior and posterior surfaces, with locations defined according to anatomical images. In a work by Adouni, muscle tendon forces were computed at six instances of the walking gait cycle, between 0% (heel strike phase) and 100% (pre-swing phase) [Adouni et al., 2012]. These six instances correspond to the instances considered for the joint reaction forces. In order to compute the forces, the orientation of the muscle tendons in Table 3.4 and the ratio to body weight values in Table 3.5 were considered.

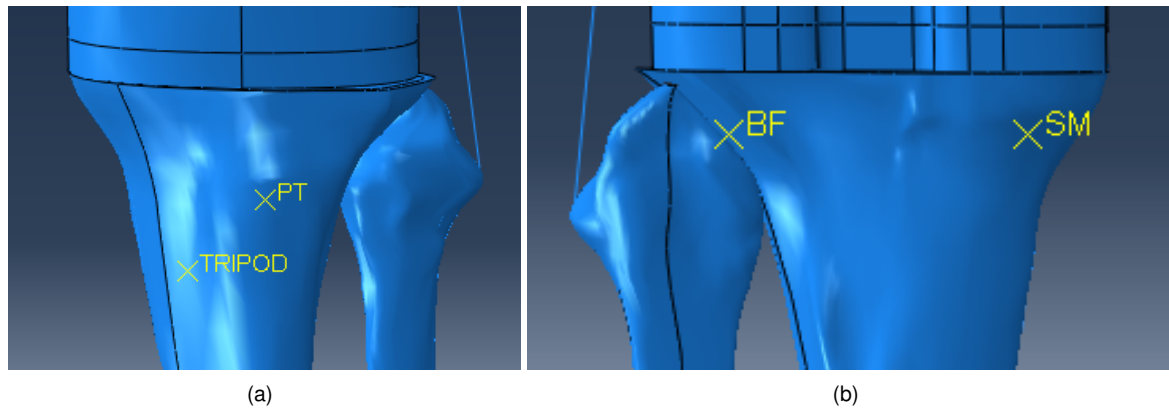


Figure 3.17: Anterior (a) and Posterior (b) views of the muscle tendon insertion sites.

Table 3.4: Orientation of the muscle tendons[Aalbersberg et al., 2005].

Muscle tendon	Frontal Orientation	Sagital Orientation
Patelar Tendon (PT)	15.9° Medial	32° Anterior
Bicep Femoris (BF)	11.8° Medial	0° Anterior
Semimembranosous (SM)	7° Lateral	16.1° Posterior
TRIPOD	7.1° Medial	18.6° Posterior

All forces are oriented according to the coordinate system shown in Figure 3.18. In Table 3.6, all forces considered for each instance of the walking gait cycle are presented.

Table 3.5: Ratio to body weight values for the six time instances of the walking gait [Adouni et al., 2012].

Muscle Tendon	Stance Phase (%)					
	0	5	25	50	75	100
PT	0.33	0.32	1.56	0.16	0	0.28
SM	0	0.37	0.09	0	0	0.28
BF	0.16	1	0.53	0.35	0.6	0
TRIPOD	0	0.37	0.18	0	0.1	0.29

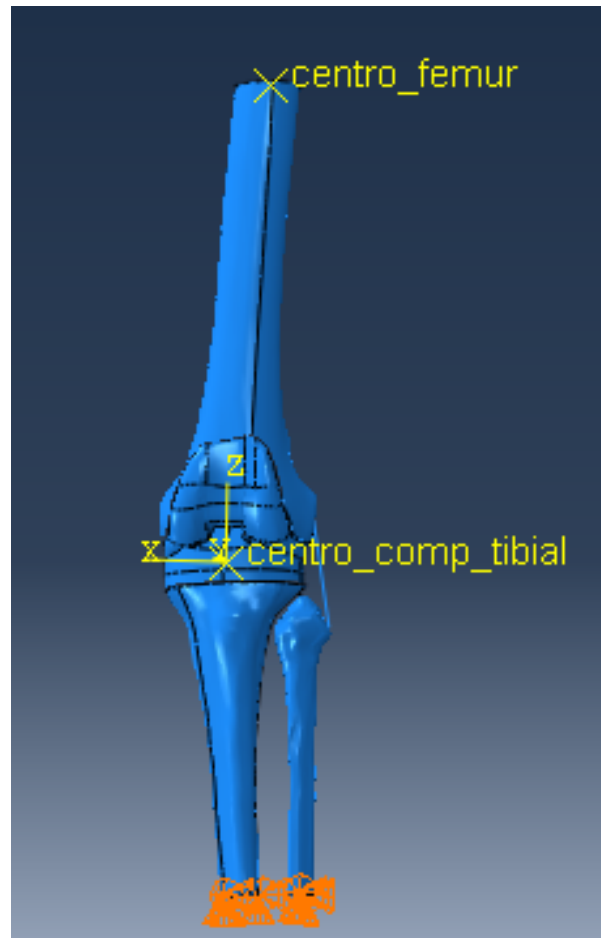


Figure 3.18: Reference point on the femoral surface where reaction forces are applied, reference point on the center of the tibial component where reaction forces are initially measured. Coordinate system used for all forces.

### 3.5.4 FE Mesh Generation

Finally, each part of the FE model was meshed. Linear Tetrahedral elements were used for all model parts, with variations in element size, as shown in Table 3.7. A convergence study was performed, where the displacement ( $U$ ) of four reference points on the femoral surface was measured for different element sizes. It was concluded that, for element sizes below 3mm, displacement values stabilized. Therefore, a size element of 2mm was considered for the femur and tibia. As for the remaining components, as they are not the focus of this study, larger element sizes were chosen to minimize com-

Table 3.6: Muscle tendon forces and reaction forces for each of the six instances of the walking gait.

Stance Phase (%)	Component	Muscle tendons forces				Reaction forces	
		PT (N)	BF (N)	SM (N)	TRIPOD (N)	Forces (N)	Moments (Nmm)
0	x	53.22	22.47	0	0	38.90	-8642.316
	y	-116.7	0	0	0	31.36	46.603
	z	186.8	107.6	0	0	-757.68	-1.764
5	x	51.61	140.4	-28.14	28.92	152.95	-7058.127
	y	-113.2	0	66.18	78.59	27.59	-21211.847
	z	181.1	672.2	229.3	232.6	-1042.32	-4143.132
25	x	251.6	77.24	-8.041	16.06	40.68	-36682.173
	y	-551.8	0	18.91	43.66	-49.20	24310.903
	z	883.1	369.7	65.52	129.2	-1490.60	-2342.517
50	x	25.8	49.15	0	0	48.46	-18591.077
	y	-56.6	0	0	0	29.46	19563.797
	z	90.57	235.3	0	0	-1356.71	2050.45
75	x	0	84.26	0	8.835	14.11	-37703.90
	y	0	0	0	24.01	-16.88	30632.123
	z	0	403.03	0	71.07	-1733.82	241.007
100	x	46.77	0	-23.32	24.1	38.84	-2222.693
	y	-102.6	0	54.83	65.49	55.43	654.28
	z	164.2	0	190	193.8	-743.30	70.92

putacional cost, in specific to minimize the duration of each simulation, as these could take between 20 and 30 minutes each. A representantion of the final FE mesh used on the models is shown in Figure 3.19. The number of nodes and elements of the FE meshes generated for each component of the numerical models, are presented in Table 3.8 and Table 3.9.

Notably, when meshing the LCL and MCL, only one element per ligament was considered. Therefore, each ligament only presented two nodes.

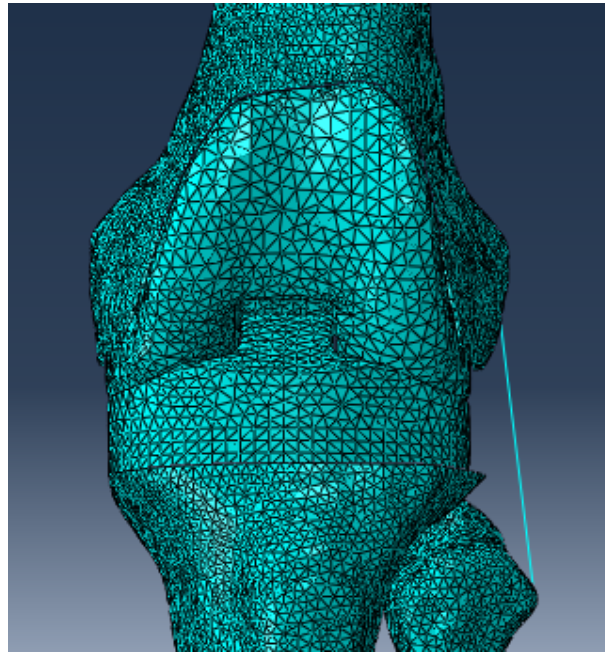


Figure 3.19: Mesh applied to the final FE knee joint model.

Table 3.7: Element size and element type used for the FE mesh applied on the numerical models of the knee bones and prosthetic components under study.

	Model Part	Approximate Element Size	Element Type
Bones	Femur	2.0	Linear Tetrahedral
	Tibia	2.0	
	Fibula	3.0	
Prosthesis	Femoral Component	3.0	Linear Tetrahedral
	Tibial Insert (Polyethylene)	2.5	
	Tibial Tray	2.5	
	Femoral Stem	3.0	Linear Tetrahedral
	Tibial Stem	2.5	

Table 3.8: Number of nodes and elements of the FE mesh generated on the numerical models of the knee bones.

	Number of Nodes/Number of Elements		
	Femur	Tibia	Fibula
Without Stems	47700/249710	26201/136244	4094/17921
Only Tibial Stem	47730/249960	25401/128372	4094/17921
Only Femoral Stem	48901/250960	26201/136244	4094/17921
With Both Stems	48901/250960	25401/128372	4094/17921

Table 3.9: Number of nodes and elements of the FE mesh generated on the numerical models of the knee prosthetic components, including both femoral and tibial stems.

Number of Nodes/Number of Elements					
	Femoral Component	Tibial Insert (Polyethylene)	Tibial Tray	Femoral Stem	Tibial Stem
Without Stems	4685/19417	2765/12422	2693/9845		
Only Tibial Stem	4480/18686	2846/10571	2707/12129		1803/7118
Only Femoral Stem	4504/18774	2693/9845	2765/12422	2594/9461	
With Both Stems	4994/20873	2860/10666	2722/12211	2594/9461	1960/8015



## Chapter 4

# Results and Discussion

As previously mentioned, the goal of this study is to assess how the insertion of an intramedullary stem influences the stresses of the complementary bone. Thus, numerical models were created, one considered a reference model, modelled after a primary TKA, and three models of different possible configurations of a revision TKA. As a simplification, the models will be referred to, in regards to their stem configuration. For example, the model with no stems is from this point on referred to as the Reference Model, and the other three are the Tibial Stem, Femoral Stem and Both Stems models. As this study is focused on the stem insertion effects on the femur, result comparisons will be focused on the Reference, Tibial Stem and Both Stems models. In Table 4.1, the prosthetic components present in each of the models are listed. Whenever possible, the same parts were used for all models, so that coherent results could be drawn. Furthermore, the same FEA parameters were applied, namely the mechanical properties, the contact and boundary conditions, the load conditions and the meshing parameters.

Finite element analysis was performed on each of the models, and biomechanical comparisons were made in order to confirm the hypothesis previously mentioned. In a previous work, Completo thoroughly analyzed the influence of different stem alternatives, in a revision TKA. In particular, he studied how different femoral stems influenced the tibia and vice-versa, in terms of stress and stability. As expected, it was concluded that stress-shielding, which is the reduction in bone density as a result of removal of stress from a bone by an implant, occurred on the femur whenever a femoral stem was used, proportional to the rigidity of the stem. Furthermore, it was also concluded that the inclusion of a tibial stem did not noticeably affect the stability of the femoral component, or of the bone/cement interface. As for the strain displayed by the femur, the changes resulting of the tibial stem insertion were considered insignificant [Completo, 2006].

### 4.1 FE Knee Joint Models

#### 4.1.1 Analysis of the Stress-Shielding Effect

A macroscopical analysis of the Von Mises stress distribution on the femur was performed, in order to confirm the stress-shielding effect resultant of the femoral stem insertion, as well as the impact

Table 4.1: Characterization of the four models analyzed and compared in this study.

Knee Joint Model	Simplified Designation	Stem Dimensions
Femoral Component		
Tibial Insert	Reference	
Tibial Tray		
Femoral Component		
Tibial Insert	Tibial Stem	14mm x 75mm
Tibial Tray		
Tibial Stem		
Femoral Component		
Tibial Insert	Femoral Stem	14mm x 125mm
Tibial Tray		
Femoral Stem		
Femoral Component		
Tibial Insert	Both Stems	14mm x 75mm
Tibial Tray		(Tibial Stem)
Tibial Stem		14mm x 125mm
Femoral Stem		(Femoral Stem)

of the tibial stem insertion.

Firstly, the stress shielding effect is addressed. According to Hooke's Law, stress is linearly dependent on a material's stiffness, or Young's Modulus, as described in Equation 4.1.

$$\sigma = E * \varepsilon \quad (4.1)$$

Since cortical bone presents a much higher Young's Modulus than trabecular bone, it is expected that larger stress values are found on the former. Thus, it is expected that the stress-shielding effect resultant of a femoral stem insertion, will mostly be visible on the cortical bone. By looking at Figure 4.1, the results obtained confirm just that. The greatest values of Von Mises stress are found along the cortical section of the diaphysis, where the cortical bone thickness is greater. In contrast, the trabecular bone presents very small Von Mises stress values, confirming that the majority of the stress is supported by the cortical bone.

Theoretically, when a stem is inserted, it is expected to absorb the stress that was being supported by the cortical bone, as a result of its material's comparatively high stiffness. When the femoral stem is included in the Both Stems model, as shown in Figure 4.2, it can be seen that, indeed, there is a decrease in the Von Mises stress on the cortical bone. It is particularly noticeable closest to the femoral distal epiphysis, where in some regions, the stress seems to have decreased in half.

#### 4.1.2 Analysis of the Von Mises Stress Distribution

Ensuing, the insertion of a tibial stem in the model was studied, again observing the femoral Von Mises stress variation. Thus, side by side comparisons of the femoral stress values were made, between

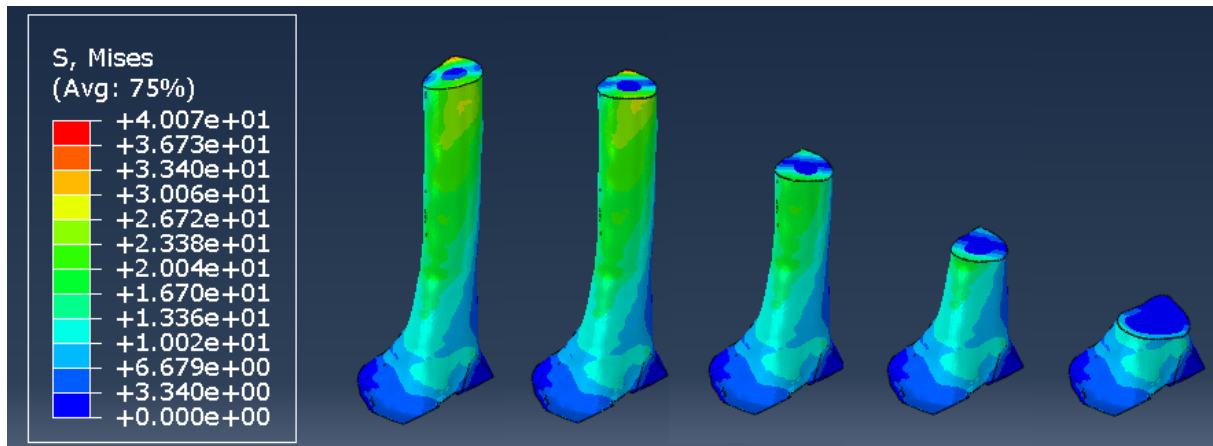


Figure 4.1: Von Mises Stress Distribution (in MPa) for Axial Cuts of the Reference Model femur, at 75% stance phase.

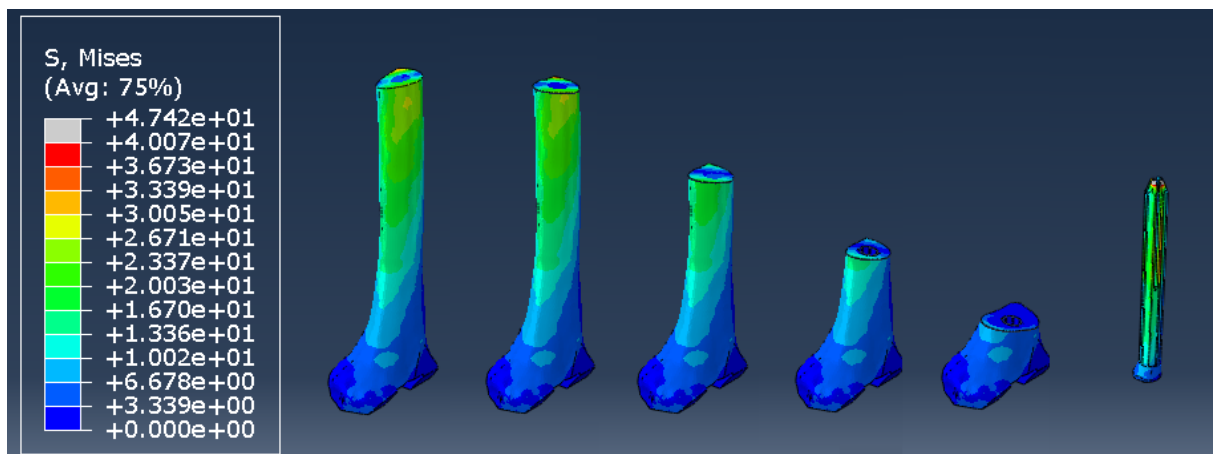


Figure 4.2: Von Mises Stress Distribution (in MPa) for Axial Cuts of the Both Stems Model femur, at 75% stance phase.

the Reference, Tibial Stem, Femoral Stem and Both Stems models. All six instances of the walking gait cycle were analyzed, in order to compare the stem influence during normal activity, as shown in Figures 4.3 to 4.8. Comparing the four models, it is possible to see a decrease on the Von Mises Stress on the cortical surface. This is particularly noticeable on the distal epiphysis region, similarly to the results obtained in Subsection 4.1.1.

Starting by comparing the Reference and Tibial Stem models, the models are a quite similar Von Mises distribution, with the changes observed macroscopically being almost none. This is observed consistently throughout the six instances analyzed. Hence, it is possible to conclude that, on this study, no significant impact on the stress distribution on the femur was observed macroscopically, as a result of a tibial stem insertion alone.

As for the models with femoral stem insertion, the Von Mises stress values decrease consistently on all six instances of the walking gait, when compared to the Reference and Tibial Stem models. Also, on both models, the decrease is very similar, although slightly more significant in the Both Stems Model. This decrease can, again, be attributed to the stress-shielding effect caused by the insertion of the femoral intramedullary stem. The similarity between the two model proves that, much like in the

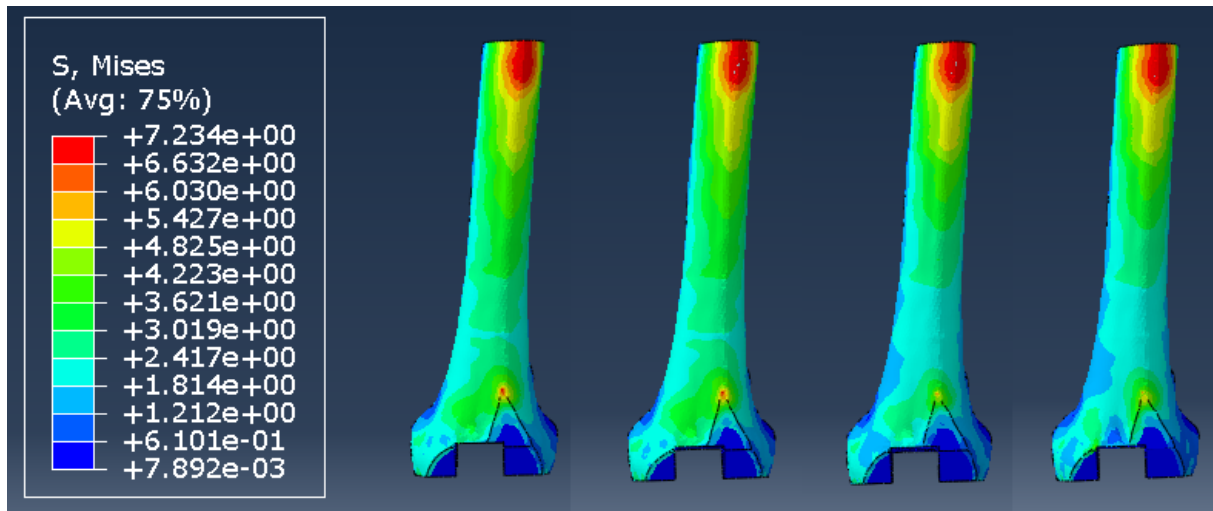


Figure 4.3: 0% Stance Phase - Comparison of the femoral Von Mises stress distribution of the Reference, Tibial Stem, Femoral Stem and Both Stems models.

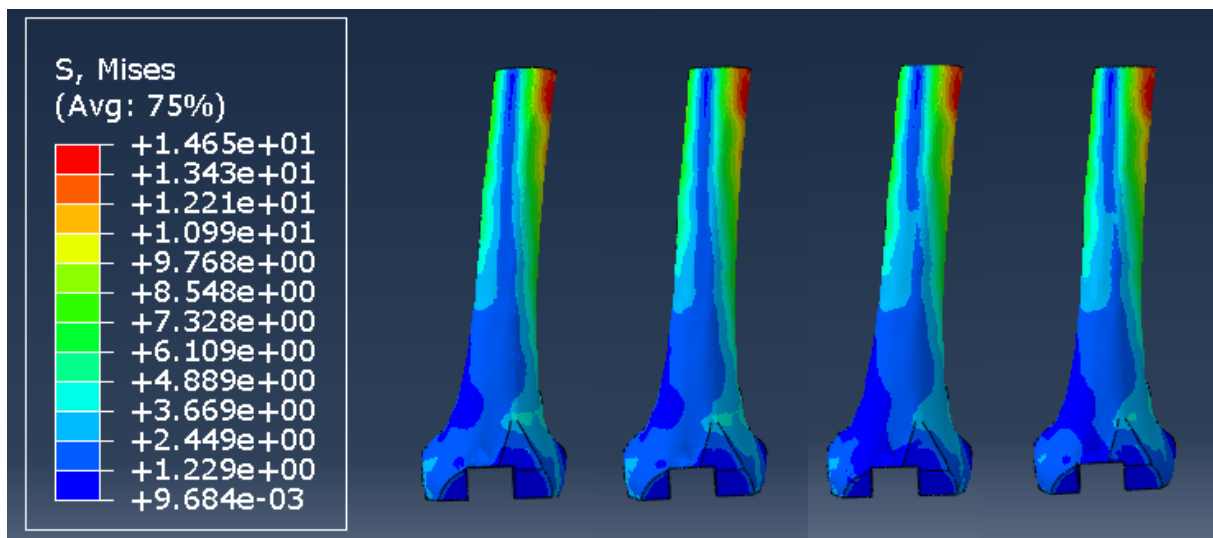


Figure 4.4: 5% Stance Phase - Comparison of the femoral Von Mises stress distribution of the Reference, Tibial Stem, Femoral Stem and Both Stems models.

previous comparison, the tibial stem influence is insignificant on the femoral stress values. While this type of analysis is enough to confirm if a decrease in the Von Mises values occurs or not, it can not quantify how significant that change is. In order to do so, a nodal analysis where the stress values of specific nodes are compared, can be used. In the following section, Section 4.2, a nodal analysis of several femoral surface nodes is performed.

## 4.2 Nodal Analysis of the FE models

So far, the FE models have been compared macroscopically, and the degree of influence of the insertion of intermedullary stems has only been assessed visually, looking at the entirety of the femur. As already mentioned, in order to complete this analysis, and to confirm the results obtained, a nodal analysis was performed. Four nodes, highlighted and shown in Figure 4.9, on different location of the

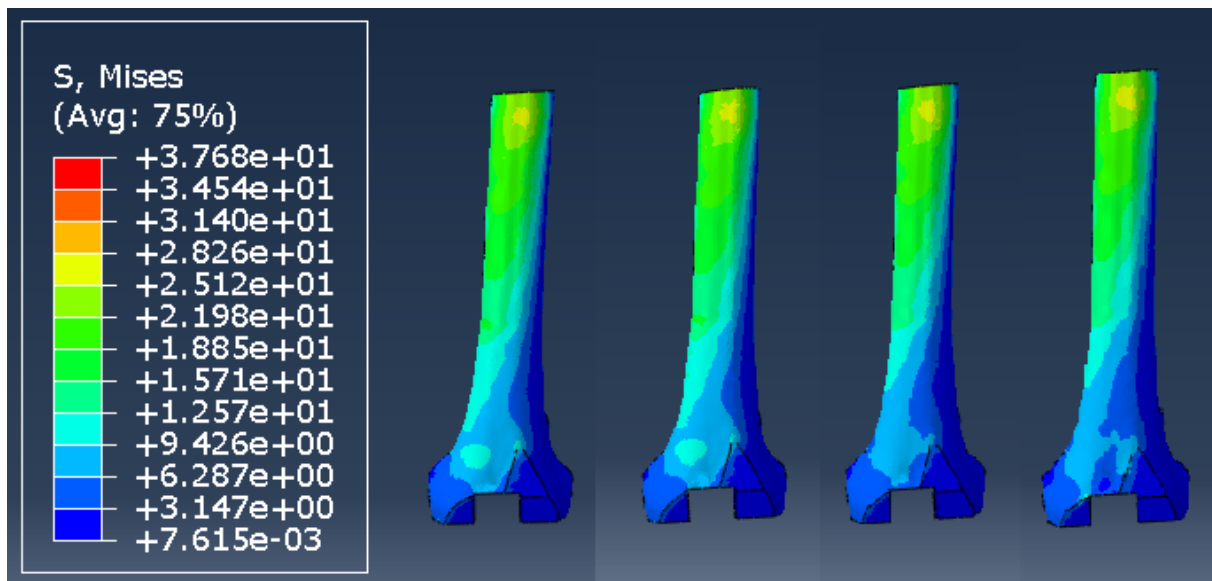


Figure 4.5: 25% Stance Phase - Comparison of the femoral Von Mises stress distribution of the Reference, Tibial Stem, Femoral Stem and Both Stems models.

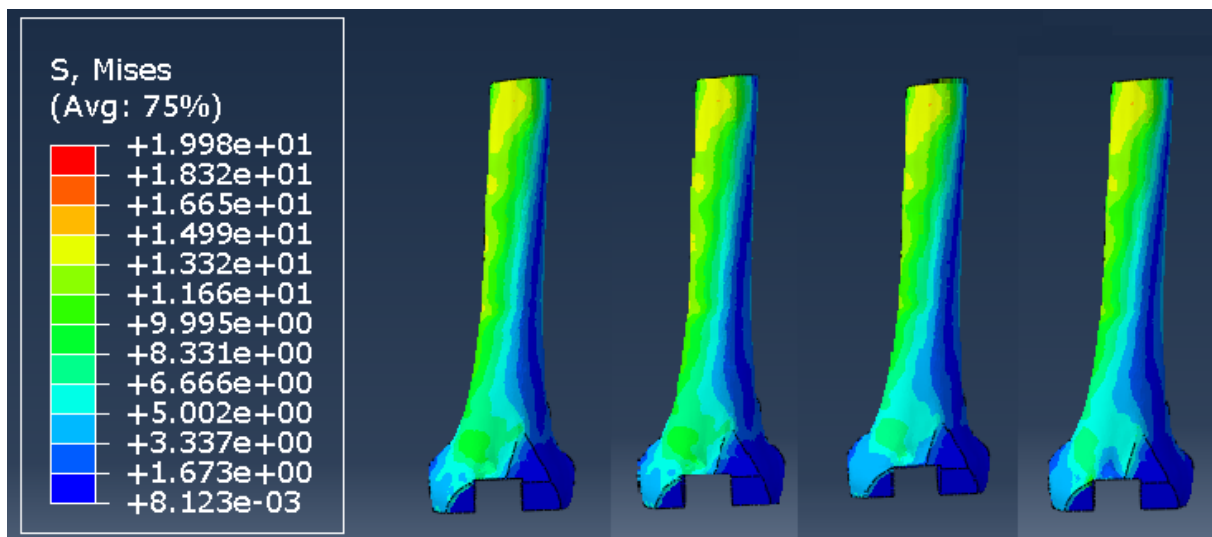


Figure 4.6: 50% Stance Phase - Comparison of the femoral Von Mises stress distribution of the Reference, Tibial Stem, Femoral Stem and Both Stems models.

femoral surface were carefully chosen to be analyzed. In the four FE models, the nodal locations were the same, whenever possible. In some cases, meshing limitations due to different bone configurations (as a result of the femoral stem insertion) did not allow for the measurement to be performed exactly on the same coordinates. In those situations, the nodes were selected as closely as possible. For the different models, the Von Mises stress values of these four nodes were obtained and compared. Again, all stance phases were considered, as previously done, and all Von Mises stress values were included in Table 4.2.

An average of the reference points' Von Mises values for each walking gait instance, of each model, was calculated, as well as an average of the stress values measured for each reference point. In order to compare the results for each model, and to quantify how much the stress values decreased,

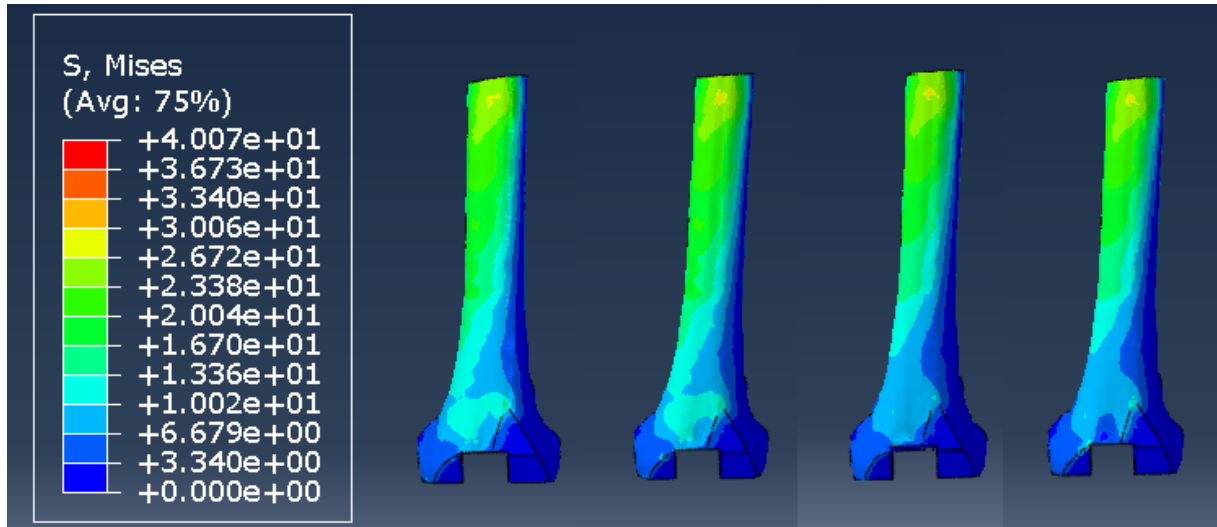


Figure 4.7: 75% Stance Phase - Comparison of the femoral Von Mises stress distribution of the Reference, Tibial Stem, Femoral Stem and Both Stems models.

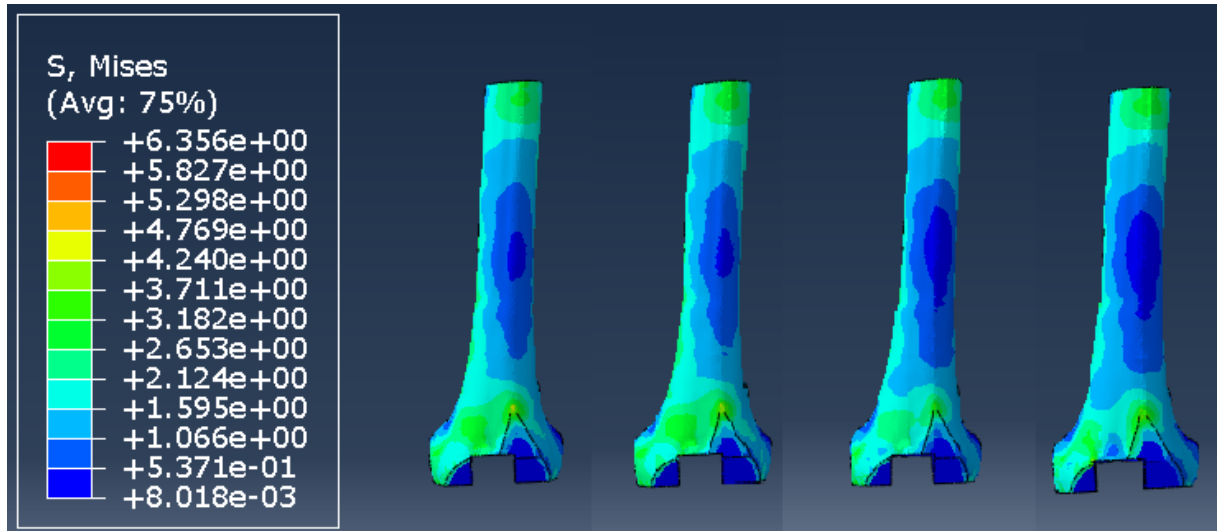


Figure 4.8: 100% Stance Phase - Comparison of the femoral Von Mises stress distribution of the Reference, Tibial Stem, Femoral Stem and Both Stems models.

the relative deviation between the nodal stress values of the Both Stems model and the nodal stress values of the Reference model, as well as between the nodal stress values of the Both Stems model and the nodal stress values of the Tibial Stem model was calculated, according to equation 4.2 and 4.3, respectively. Relative deviation between other model comparisons were not included, as the values of the Reference and Tibial Stem models are quite similar, and therefore would present very small deviations. As for the Femoral Stem model, it was not calculated as it was not a primary interest of this study, and also because the values are very similar to the Both Stems model. All results are included in Tables 4.3 and 4.4.

$$\text{Relative Deviation (Both Stems - Reference)} = \frac{\sigma_{bs} - \sigma_r}{\sigma_r} * 100 \quad (4.2)$$

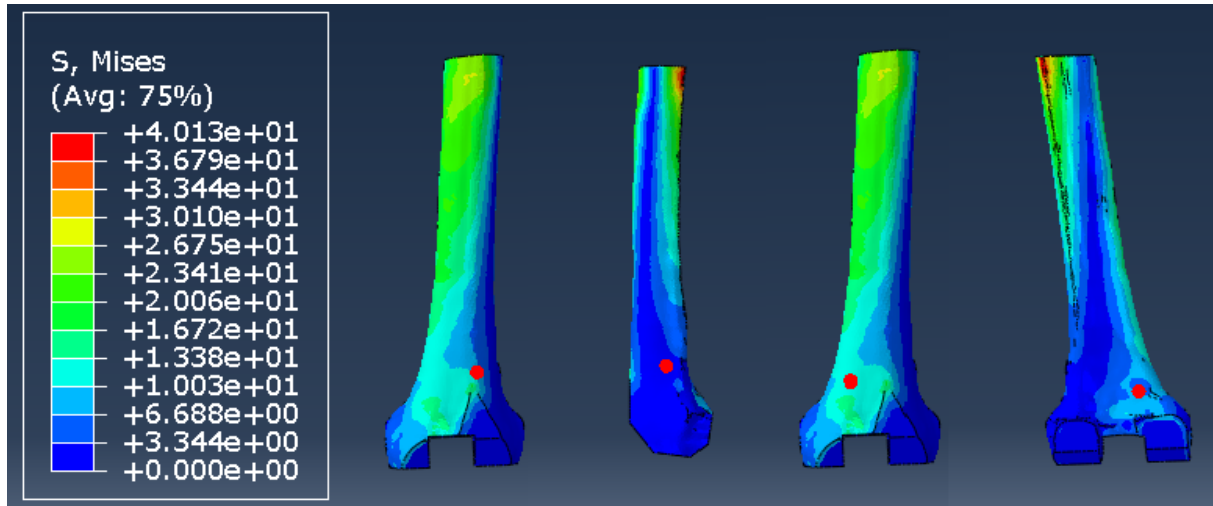


Figure 4.9: Highlighted representation (red dots) of the femoral surface nodes (1 to 4) chosen for analysis.

$$Relative\ Deviation\ (Both\ Stems - Tibial\ Stem) = \frac{\sigma_{bs} - \sigma_{ts}}{\sigma_{ts}} * 100 \quad (4.3)$$

In Table 4.3, the average Von Mises stress between the four nodes analyzed, for each gait cycle instant considered is presented. Firstly, a comparison of the values between different instances with the results obtained in Subsection 4.1.2 is made. The results are consistent, as the highest stress values are obtained in the same instances as in the previous subsection. Comparing the values obtained between models, the Reference Model and the Tibial Stem Model present very similar average values, with residual relative standard deviations, all below 4%. Therefore, it is safe to conclude that the tibial stem insertion did not affect the Von Mises stress values of the selected nodes.

As for the Both Stems Models, in all the instances considered, the nodal stress values decreased, in comparison with the models previously mentioned. While in Table 4.2, the decrease is not always consistent, with some nodes presenting a more significant difference than others, it is clear to see on Table 4.3, that for all instances, the average Von Mises decreases consistently on the Both Stems Model. As for the relative deviation results, when comparing the Both Stems model and the Reference Model, the average decreases between 13% and 24%. For the Tibial Stem model comparison, the deviation is quite similar, with decreases between 11% and 23%.

Moreover, the results obtained when considering for each reference point, the average between all six instances, are coherent with the results obtained thus far. The results obtained for the Reference and Tibial Stem models are, again, quite similar, with very small deviations. The deviations between the Both Stems and the Reference model are between 10 and 25%, as are the deviations between the Both Stems and the Tibial Stem model. Similarly to before, these results indicate a relation between the insertion of the femoral stem with a decrease in stress values in the femur, while the tibial stem insertion does not have a significant effect on them.

Table 4.2: Von Mises stress values of four nodes of the femur surface, for each of the models (Reference, Tibial Stem, Femoral Stem and Both Stems).

Stance Phase	Node	Von Mises Stress (MPa)			
		Reference	Tibial Stem	Femoral Stem	Both Stems
0	1	3.63278	3.60151	2.91811	2.9489
	2	1.40962	1.41835	1.2238	1.19459
	3	2.38	2.39981	1.90766	1.73112
	4	1.54409	1.45293	1.21775	1.25276
5	1	2.64564	2.66765	2.38103	2.38969
	2	3.89916	3.9155	3.42745	3.47322
	3	0.924481	0.934064	0.893084	0.855153
	4	3.18054	3.03061	2.5206	2.58886
25	1	5.60927	5.39326	3.96183	4.08619
	2	2.44786	2.4256	2.24103	2.29297
	3	8.65965	8.6664	6.88126	6.42412
	4	5.25233	4.97732	4.06556	3.92101
50	1	3.77311	3.62041	2.82994	3.00315
	2	2.02364	2.00152	1.84159	1.84669
	3	7.32648	7.154109	5.94769	5.49277
	4	4.56471	4.33138	3.60664	3.55132
75	1	7.68161	7.45027	5.6273	5.78294
	2	2.42458	2.3911	2.16856	2.19964
	3	9.96286	9.98414	7.93556	7.38292
	4	5.0011	4.7256	3.81503	3.71648
100	1	2.21374	2.19233	1.84177	1.87626
	2	1.25591	1.26663	1.11144	1.11183
	3	1.94474	1.95523	1.59842	1.43684
	4	1.97012	1.86989	1.60137	1.62626

### 4.3 Influence of changes in the Trabecular Bone Stiffness on the Nodal Von Mises Stress Values

Changes to the model's parameters were made, namely different Young's Modulus values were attributed to the trabecular bone. These alterations were studied in order to confirm the results previously obtained, by determining whether the stresses were being correctly distributed to the cortical bone. Since the intermedullary stems are in contact with not only cortical bone, but also trabecular bone, an incorrect transfer of the stresses to the trabecular bone could occur, due to its much lower Young's Modulus. The models were analyzed with two different trabecular  $E$  values.

Firstly, a Young's Modulus of  $E = 3\text{GPa}$  was considered, corresponding to the stiffness considered for the interaction simulating the bone cement connecting the femur and femoral component. Secondly, a Young's Modulus of  $E = 17\text{GPa}$  was considered, in order to study how the results would be affected,

Table 4.3: Average Von Mises stress values between the four reference points, for each stance phase percentage, of each model. Relative Deviation between the average Von Mises stress values calculated for the Both Stems model, and the Reference and Tibial Stem models.

Stance Phase	Average Von Mises Stress (MPa)				Relative Deviation of the BS Model (%)	
	Reference	Tibial Stem	Femoral Stem	Both Stems	Reference	Tibial Stem
0	2.24	2.22	1.82	1.78	-21	-19.7
5	2.66	2.64	1.81	2.33	-13	-11.8
25	5.49	5.37	4.29	4.17	-24	-22.3
50	4.42	4.28	3.56	3.47	-21	-18.8
75	6.27	6.14	4.89	4.77	-24	-22.3
100	1.85	1.82	1.54	1.51	-18	-16.9

Table 4.4: Average Von Mises stress values of all stance phase percentage considered, for each reference point. Relative Deviation between the average Von Mises stress values calculated for the Both Stems model, and the Reference and Tibial Stem models.

Ref Point	Average Von Mises Stress (MPa)				Relative Deviation of the BS Model (%)	
	Reference	Tibial Stem	Femoral Stem	Both Stems	Reference	Tibial Stem
1	4.26	4.15	3.26	3.35	-21	-19.4
2	2.24	2.24	1.67	2.01	-10	-10
3	5.20	5.18	4.19	3.89	-25	-24.9
4	3.59	3.40	2.80	2.78	-23	-18.3

considering a uniform bone stiffness for the entire bone.

#### 4.3.1 Trabecular Bone with Young's Modulus of 3GPa

For the models considering the trabecular bone  $E = 3\text{GPa}$ , the Von Mises nodal stress values were calculated, for the same nodes referenced in Section 4.2. The average values for each instance and for each node, as well as the relative standarddeviations between models are presented in Tables 4.5 and 4.6, respectively.

Comparing the average results of these models, with the results previously obtained in Section 4.2, the average Von Mises stress values of the cortical surface nodes, decrease when the trabecular bone is considered at 3GPa. This means that, considering a stiffer trabecular bone, it will support greater stress values, transferring less to the cortical bone surface.

As for the relative deviations, in all cases there is a decrease in the stress values for the Both Stems Model, when compared to the Reference and Tibial Stem models. When compared with the Reference model, the stress decrease percentage is between 15 and 29%, for the average for each instance, and it is between 4 and 37%, when comparing the average for each reference point. As for

Table 4.5: Trabecular bone stiffness at 3GPa - Average Von Mises stress values between the four reference points, for each stance phase percentage, of each model. Relative Deviation between the average Von Mises stress values calculated for the Both Stems model, and the Reference and Tibial Stem models.

Stance Phase	Average Von Mises Stress (MPa)				Relative Deviation of the BS Model (%)	
	Reference	Tibial Stem	Femoral Stem	Both Stems	Reference	Tibial Stem
0	1.81	1.80	1.31	1.28	-29	-28.5
5	2.13	2.11	1.80	1.81	-15	-14.5
25	4.53	4.45	3.30	3.26	-28	-26.8
50	3.63	3.56	2.76	2.73	-25	-23.5
75	5.15	5.06	3.73	3.69	-28	-27.1
100	1.45	1.43	1.06	1.04	-28	-27.2

the Tibial Stem model comparison, the relative deviation is similar, between 14 and 28%, and between 4 and 35%, for each case, respectively.

Table 4.6: Trabecular bone stiffness at 3GPa - Average Von Mises stress values of all walking gait instances considered, for each reference point. Relative Deviation between the average Von Mises stress values calculated for the Both Stems model, and the Reference and Tibial Stem models.

Ref Point	Average Von Mises Stress (MPa)				Relative Deviation of the BS Model (%)	
	Reference	Tibial Stem	Femoral Stem	Both Stems	Reference	Tibial Stem
1	3.35	3.26	2.10	2.12	-37	-35
2	2.06	2.05	1.94	1.97	-4	-4.2
3	4.52	4.53	3.34	3.16	-30	-30.4
4	2.54	2.43	1.92	1.96	-23	-19.3

### 4.3.2 Trabecular Bone with Young's Modulus of 17GPa

As for the models with trabecular bone stiffness at 17GPa, the stress averages decreased as well, for all the cases considered. Hence, the trabecular bone supports an even greater amount of stress, as it was expected. Again, the nodal stresses measured for the Both Stems model are lower than the ones measured for the Reference model, decreasing between 2 and 33%, for the averages of each instance, and between 0 and 41%, for the averages of each reference point. Similar results were obtained in comparison with the Tibial Stem model, with respective decreases between 1.4 and 33%, and between 0 and 40%. All results are shown in Tables 4.7 and 4.8.

After analyzing the models with different trabecular bone stiffness values, and comparing them to the original model, with a Young's Modulus of  $E = 1\text{GPa}$ , it is possible to conclude that cortical surface stress is inversely proportional to trabecular bone stiffness. This results from the fact that a stiffer

Table 4.7: Trabecular bone stiffness at 17GPa - Average Von Mises stress values between the four reference points, for each stance phase percentage, of each model. Relative Deviation between the average Von Mises stress values calculated for the Both Stems model, and the Reference and Tibial Stem models.

Stance Phase	Average Von Mises Stress (MPa)				Relative Deviation of the BS Model (%)	
	Reference	Tibial Stem	Femoral Stem	Both Stems	Reference	Tibial Stem
0	0.84	0.84	0.59	0.58	-31	-31
5	1.0	1.0	-	0.98	-2	-1.4
25	2.35	2.33	1.76	1.74	-26	-25.2
50	1.81	1.80	1.48	1.47	-19	-18.3
75	2.68	2.65	2.01	1.99	-26	-25.1
100	0.59	0.59	0.41	0.39	-33	-33

Table 4.8: Trabecular bone stiffness at 17GPa - Average Von Mises stress values of all walking gait instances considered, for each reference point. Relative Deviation between the average Von Mises stress values calculated for the Both Stems model, and the Reference and Tibial Stem models.

Ref Point	Average Von Mises Stress (MPa)				Relative Deviation of the BS Model (%)	
	Reference	Tibial Stem	Femoral Stem	Both Stems	Reference	Tibial Stem
1	1.48	1.44	0.92	0.87	-41	-39.9
2	1.37	1.37	1.3	1.37	0	0
3	2.53	2.53	2.11	1.86	-27	-26.7
4	0.81	0.79	0.67	0.67	-18	-15.7

trabecular bone will absorb greater amounts of stress, as expected through Hooke's Law. As for the comparisons between different models, stem configuration wise, the relative deviations remained similar for the different  $E$  values considered. Thus, the model studied with trabecular bone stiffness  $E = 1\text{GPa}$ , can be considered adequate for the study of Von Mises stress distribution to the cortical surface.



## Chapter 5

# Conclusions

In this chapter, a summary of the main conclusions drawn from the results presented in Chapter 4 is presented. Additionally, a critical analysis of the short-comings of this study and a list of improvements for possible future works are also included.

### 5.1 Main conclusions

The main goal of this work was to assess whether a stem insertion, typically used for revision TKAs, influences the stresses on the complementary bone. For that, finite element analysis was used and four different knee joint models were created, representing a primary surgery case, and three different possible revision surgery configurations.

In order to create these models, CT images of a knee were used as a basis for the creation of the bone models, while the prosthetic components were modelled based on scanings of real components. The model was assembled using a CAD software program, and in the finite element analysis software, the mechanical properties of the materials of each component, the interactions and contacts, the loading conditions and the mesh were defined.

Firstly, the Von Mises stress distribution was analyzed on a macroscopical level for each of the model configurations. Firstly, this analysis was used to confirm the stress-shielding effect on the femur as a result of a femoral stem insertion. Secondly, femoral stress distributions of the four models were compared side by side, to detect variations from the reference model. In this, the insertion of a tibial stem was determined to not affect in a significant manner, the stress distribution, when compared to the reference model.

Then, a nodal analysis was performed, in which four nodes of the femoral mesh were chosen and their Von Mises stress values were collected, and compared between models. In order to easily compare the data, two different methods were used. Firstly, the average value of the four nodes was measured, for each instance, and for each model. Secondly, the average of the six instances considered was measured, for each reference point, and for each model. Furthermore, the relative standard deviations between the Both Stems model and the Reference Model, and between the Both Stems model and the

Tibial Stem model, were determined. Again, no significant differences were obtained, as a result of the tibial stem insertion. As for the femoral stem influence, a stress value decrease between 10 and 25% was registered for each case considered.

Finally, different Young's Modulus values for the trabecular bone were tested, namely  $E$  was altered to 3GPa and 17GPa. When comparing with the results of the initial value of 1GPa, all results were consistent. The tibial stem insertion did not produce significant impact in the Von Mises nodal stress values, and the femoral stem insertion caused a decrease in the femoral stress values, due to the stress shielding effect.

After analysing the results, one can conclude that the insertion of a tibial stem does not significantly affect the stress distribution on the femur, for both a macroscopical analysis of the Von Mises stress distribution, and a nodal analysis of various nodal points on the femoral surface. However, when a femoral stem is introduced, the Von Mises stress magnitude on the femur decreases, as expected, thus confirming the stress shielding effect resultant of the insertion of a titanium stem. These results are aligned with the work of Completo, who determined that, although the use of a tibial stem can decrease the femur/femoral component interface stability, the effects on the femoral strain are insignificant [Completo, 2006].

## 5.2 Short-comings, Improvements and Future Work

In this section, a critical analysis of the limitations of this studied is done. The examples discussed can also be considered as suggestions of issues to keep in mind, in future works exploring the same topic.

Firstly, the bones went through a simplification process during the geometrical modelling phase. After the segmentation process, previous works imported the files to a CAD software and the modelling of the bones was performed according to these results. In this particular study, the bones were modelled as approximated solid bodies, in order to simplify the meshing of these parts. Due to this, an accurate distribution of the bone density values was sacrificed, as it was no longer possible to use the information of the CT images to transform Hounsfield Unit values into apparent density values. Thus, the bones were divided into linear, isotropic and homogeneous portions of cortical and trabecular bone, with Young's Modulus values of 17GPa and 1GPa, respectively.

Evidently, this simplified model does not accurately reflect the stress distribution on the bones, with or without stems included, as stress values are directly correlated with the value of the Young's modulus, according to Hooke's Law. Therefore, most certainly, the stress values obtained are not as accurate as they would be if the bone density values were calculated from the CT image information.

Secondly, when creating the simplified bone models, the trabecular portion was modelled by off-setting the full solid body bone model. When performing these offsets, the theoretical cortical thickness of the bones was followed as much as possible. Theoretically, the stem is introduced inside the inter-medullary canal, and its tip will, at some point, contact cortical bone and become completely surrounded by it. Nevertheless, it is virtually impossible to represent this interaction absolutely perfectly. Since an

approximation was considered, it was not possible to recreate this ideal scenario. The stem tips do contact cortical bone, but they do so intermittently with trabecular bone. It is possible that, due to this contact with the trabecular bone, with a much lower stiffness, the stem was not able to support the correct load it would have in an ideal situation. Therefore, the stress values on the cortical surface of the femur could have possibly decreased even more, had the stem tip been completely in contact with cortical bone.

Furthermore, when performing nodal analysis, nodes from each model's mesh are considered. Evidently, stem insertion alters the bone parts, resulting in different meshes being applied. Thus, some of the nodes considered, not all, presented slight coordinate differences between models. As a result, the difference between stress values obtained may have been influenced by these differences.

Finally, due to meshing limitations, only nodes on the femoral surface were available to analyze. If it had been possible, analyzing the Von Mises stress of interior points on the femur, closer to the intermedullary canal and the stem would have been of interest for this type of work.



# Bibliography

- S. Aalbersberg, I. Kingma, J. L. Ronsky, R. Frayne, and J. H. Van Dieën. Orientation of tendons in vivo with active and passive knee muscles. *J Biomech*, 38(9):1780–1788, 2005. DOI: 10.1016/j.jbiomech.2004.09.003.
- J. F. Abulhasan and M. J. Grey. Anatomy and physiology of knee stability. *J Funct Morphol Kinesiol*, 2(34), September 2017. DOI: 10.3390/jfmk2040034.
- M. Adouni, A. Shirazi-Adl, and R. Shirazi. Computational biodynamics of human knee joint in gait: From muscle forces to cartilage stresses. *J Biomech*, 45(12):2149–2156, 2012. DOI: 10.1016/j.jbiomech.2012.05.040.
- S. Affatato. *Surgical Techniques in Total Knee Arthroplasty (TKA) and Alternative Procedures*. 2015. ISBN 9781782420385.
- T. Bergmann and D. Peterson. *Chiropractic Technique: Principles and Procedures*. Mosby, 2011. ISBN: 9780323080569.
- J. J. Cherian, B. H. Kapadia, S. Banerjee, J. J. Jauregui, K. Issa, and M. A. Mont. Mechanical, anatomical, and kinematic axis in tka: Concepts and practical applications. *Curr Rev Musculoskelet Med*, 7(2):89–95, Jun 2014. DOI: 10.1007/s12178-014-9218-y.
- H. J. Cho and D. S. Kwak. Mechanical properties and characteristics of the anterolateral and collateral ligaments of the knee. *Applied Sciences*, 10(18), 2020. DOI: 10.3390/app10186266.
- A. Completo. *Estudo Numérico e Experimental da Biomecânica da Prótese do Joelho*. PhD thesis, Universidade de Aveiro, Departamento de Engenharia Mecânica, 2006.
- DePuy. Sigma Fixed Bearing Knees: Function with Wear Resistance, 2010.
- DePuy. Sigma Fixed Bearing Knee System: Value Brief, 2012.
- DePuy. Sigma Revision and M.B.T. Revision Tray Surgical Technique, 2013.
- DePuy. Sigma Primary Knee System: Balanced Surgical Technique, 2014.
- DePuy. Sigma: Knee Revision Reference Cards, 2017.
- B. H. Derrickson and G. J. Tortora. *Principles of anatomy and physiology*. John Wiley Sons, Inc., 15th edition, 2017. ISBN: 978-1-119-41482-7.

- B. Eidel, A. Gote, C. P. Fritzenb, A. Ohrndorf, and H. J. Christ. Tibial implant fixation in tka worth a revision? – how to avoid stress-shielding even for stiff metallic implants. *Computer Methods in Biomechanics and Biomedical Engineering*, September 2020. DOI: 10.1080/10255842.2020.1830274.
- S. D. Ganvir, S. Ganvir, and A. Nagarale. *Biomechanics of Joints*. Jaypee Brothers Medical Publishers, 1st edition, 2013. ISBN: 9789350904947, DOI: 10.5005/jp/books/11797<sub>8</sub>.
- M. J. George. Valgus deformity correction in total knee replacement: An overview. *InTech Open*, 2019. DOI: 10.5772/intechopen.89739.
- V. D. Graaff. *Human Anatomy*. McGraw-Hill Education, 6th edition, 2001. ISBN: 0072849185.
- J. P. Halloran, A. J. Petrella, and P. J. Rullkoeter. Explicit finite element modeling of total knee replacement mechanics. *Journal of Biomechanic*, 38:323–331, 2005. DOI: 10.1016/j.jbiomech.2004.02.046.
- W. Hasemkamp. Flexible micro/nanofabricated systems for medical devices and implants, 2013.
- A. D. Heiner. Structural properties of fourth-generation composite femurs and tibias. *J Biomech*, 41: 3282–4, August 2008. DOI: 10.1016/j.jbiomech.2008.08.013.
- J. J. Hermans, A. Beumer, T. A. W. Jong, and G. J. Kleinrensink. Anatomy of the distal tibiofibular syndesmosis in adults: a pictorial essay with a multimodality approach. *J. Anat.*, (217):633–645, 2010. DOI: 10.1111/j.1469-7580.2010.01302.x.
- M. C. S. Inacio, E. W. Paxton, S. E. Graves, R. S. Namba, and S. Nemes. Projected increase in total knee arthroplasty in the united states – an alternative projection model. *Osteoarthritis and Cartilage*, 25(11): 1797–1803, 2017. DOI: <https://doi.org/10.1016/j.joca.2017.07.022>.
- P. Indelli, M. Marcucci, A. Graceffa, S. Charlton, and L. Latella. Primary posterior stabilized total knee arthroplasty: analysis of different instrumentation. *J Orthop Surg Res*, 9(54), 2014. DOI: 10.1186/s13018-014-0054-y.
- E. Jämsen, P. Jäntti, T. Puolakka, and A. Eskelinen. Primary knee replacement for primary osteoarthritis in the aged: gender differences in epidemiology and preoperative clinical state. *Aging Clin Exp Res*, 24 (6):691–698, December 2012. DOI: 10.3275/8592.
- K. Kang, T. Tien, M. C. Lee, K.-Y. Lee, B. Kim, and D. Lim. Suitability of metal block augmentation for large uncontained bone defect in revision total knee arthroplasty (tka). *Journal of Clinical Medicine*, 8:384, March 2019. DOI: 10.3390/jcm8030384.
- R. Kattimani. Component alignment in total knee replacement. *Ortho and Rheum Open Access Journal*, 11(3):1–3, April 2018. DOI: 10.19080/oroaj.2018.11.555815.
- H. Kim, R. Pelker, D. Gibson, J. Irving, and J. Lynch. Rollback in posterior cruciate ligament-retaining total knee arthroplasty: A radiographic analysis. *The Journal of Arthroplasty Vol. 12 No. 5*, 12(5):553–61, August 1997. DOI: 10.1016/s0883-5403(97)90179-0.

- H. Kim, S. Kim, Y. Seo, S. Choi, Y. Seong, H. D., and Z. Y. The epidemiology of total knee replacement in south korea: national registry data. *Rheumatology (Oxford)*, 47(1):88–91, January 2008. DOI: 10.1093/rheumatology/kem308.
- S. Kim, S. Gaiser, and J. Meehan. Epidemiology of primary hip and knee arthroplasties in germany: 2004 to 2008. *The Journal of Arthroplasty*, 27(10):1777–1782, December 2012. DOI: 10.1016/j.arth.2012.06.017.
- D. Klues. Finite element analysis in orthopaedic biomechanics. In *Finite Element Analysis*, chapter 6. IntechOpen, 2010. DOI: 10.5772/intechopen.83980.
- I. Kutzner, B. Heinlein, F. Graichen, A. Bender, A. Rohlmann, A. Halder, A. Beier, and G. Bergmann. Loading of the knee joint during activities of daily living measured in vivo in five subjects. *Journal of Biomechanics*, 43:2164–2172, 2010. DOI: 10.1016/j.jbiomech.2010.03.046.
- R. LaPrade, T. Ly, F. Wentorf, and L. Engebretsen. The posterolateral attachments of the knee a qualitative and quantitative morphologic analysis of the fibular collateral ligament, popliteus tendon, popliteofibular ligament, and lateral gastrocnemius tendon\*. *The American Journal of Sports Medicine*, 31:854–60, 11 2003. DOI: 10.1177/03635465030310062101.
- P. C. Liacouras and J. S. Wayne. Computational modeling to predict mechanical function of joints: Application to the lower leg with simulation of two cadaver studies. *J Biomech Eng*, 129(6):811, 2007. DOI: 10.1115/1.2800763.
- F. Liu, B. Yue, H. R. Gadikota, M. Kozanek, W. Liu, T. J. Gill, H. E. Rubash, and G. Li. Morphology of the medial collateral ligament of the knee. *J Orthop Surg Res*, 5(69), 2010. DOI: 10.1186/1749-799X-5-69.
- E. Losina, T. Thornhill, B. Rome, J. Wright, and J. Katz. The dramatic increase in total knee replacement utilization rates in the united states cannot be fully explained by growth in population size and the obesity epidemic. *J Bone Joint Surg Am*, 94(3):201–207, February 2012. DOI: 10.2106/JBJS.J.01958.
- K. Malizos and S. Varitimidis. Infection in total knee arthroplasty. *Management of Periprosthetic Joint Infections*, pages 133–156, January 2017. DOI: 10.1016/B978-0-08-100205-6.00007-0.
- P. Mansfield and D. Neumann. *Essentials of Kinesiology for the Physical Therapist Assistant*. Mosby, 2018. ISBN: 9780323544993.
- M. C. Moreira. Analysis of the bone stresses for a posterior stabilized knee prosthesis with an endomedullary stem. Master’s thesis, Instituto Superior Técnico, 2018.
- G. A. Orozco, P. Tanska, M. E. Mononen, K. S. Halonen, and R. K. Korhonen. The effect of constitutive representations and structural constituents of ligaments on knee joint mechanics. *Scientific Reports*, 8 (1), 2018. DOI: 10.1038/s41598-018-20739-w.
- S. Putman, J. N. Argenson, P. Bonnevalle, M. Ehlinger, P. Vie, S. Leclercq, B. P., S. Lustig, S. Parratte, N. Ramdane, and M. Colmar. Ten-year survival and complications of total knee

- arthroplasty for osteoarthritis secondary to trauma or surgery: A french multicentre study of 263 patients. *Orthopaedics Traumatology: Surgery Research*, 104(2):161–164, 2018. DOI: <https://doi.org/10.1016/j.otsr.2017.11.019>.
- J. Reddy. *An Introduction to the Finite Element Method*. McGraw-Hill Education, 3th edition, 2005. ISBN: 9780071244732.
- N. S. Ribeiro, P. C. Fernandes, D. S. Lopes, J. O. Folgado, and P. R. Fernandes. 3-D solid and finite element modeling of biomechanical structures - a software pipeline. *7th EUROMECH Solid Mechanics Conference*, 1 2009.
- T. J. Robalo. Analysis of bone remodeling in the tibia after total knee prosthesis. Master's thesis, Instituto Superior Técnico, 2011.
- O. Robertson, S. Bizjajeva, A. M. Fenstad, O. Furnes, L. Lidgren, F. Mehnert, A. Odgaard, A. B. Pedersen, and L. I. Havelin. Knee arthroplasty in denmark, norway and sweden: A pilot study from the nordic arthroplasty register association. *Acta Orthopaedica*, 81(1):82–89, January 2010. DOI: 10.3109/17453671003685442.
- J. C. Ryan and J. L. Williams. Tensile testing of rodlike trabeculae excised from bovine femoral bone. *J Biomech*, 22(4):351–5, 1989. DOI: 10.1016/0021-9290(89)90049-3.
- C. E. H. Scott and L. C. Biant. The role of the design of tibial components and stems in knee replacement. *J. Bone Joint Surg. Br.*, 94(8):1009–1015, 2012. DOI: 10.1302/0301-620X.94B8.28289.
- B. D. Shannon, J. F. Klassen, J. A. Rand, D. J. Berry, and R. T. Trousdale. Revision total knee arthroplasty with cemented components and uncemented intramedullary stems. *The Journal of Arthroplasty*, 18(7): 27–32, 2003. DOI: 10.1054/S0883-5403(03)00301-2.
- L. Sharma, J. Song, D. Felson, S. Cahue, E. Shamiyeh, and D. Dunlop. The role of knee alignment in disease progression and functional decline in knee osteoarthritis. *JAMA*, 286(2):188–95, July 2001. DOI: 10.1001/jama.286.2.188.
- E. Song, J. Seon, M. J., and J. Yim. The evolution of modern total knee prostheses. *InTech Open*, February 2013. DOI: 10.5772/54343.
- H. Tateishi. Indications for total knee arthroplasty and choice of prosthesis. *JMAJ*, 44(4):153–158, 2001.
- D. Tigani, S. Comitini, and D. Leonetti. *Revision total knee arthroplasty (TKA)*, chapter 14, pages 229–242. *Surgical Techniques in Total Knee Arthroplasty (TKA) and Alternative Procedures*, 2015. ISBN: 9781782420385.
- R. Vaishya, M. Chauhan, and A. Vaish. Bone cement. *J Clin Orthop Trauma*, 4(4):157–163, December 2013. DOI: 10.1016/j.jcot.2013.11.005.
- C. Van Putte, J. Regan, and A. Russo. *Seeley's Essentials of Anatomy and Physiology*. McGraw-Hill Education, 9th edition, 2016. ISBN: 9780078097324.

- M. Viceconti, R. Muccini, M. Bernakiewicz, M. Baleani, and L. Cristofolini. Large-sliding contact elements accurately predict levels of bone-implant micromotion relevant to osseointegration. *Journal of Biomechanics*, 33:1611–1618, 2000. DOI: 10.1016/S0021-9290(00)00140-8.
- P. A. Yushkevich, J. Piven, C. Hazlett, H. Smith, G. Smith, R. Ho, S. Ho, J. C. Gee, and G. Gerig. User-guided 3D active contour segmentation of anatomical structures: Significantly improved efficiency and reliability. *Neuroimage*, 31(3):1116–1128, 2006. DOI: 10.1016/j.neuroimage.2006.01.015.

